General Disclaimer

One or more of the Following Statements may affect this Document

- This document has been reproduced from the best copy furnished by the organizational source. It is being released in the interest of making available as much information as possible.

- This document may contain data, which exceeds the sheet parameters. It was furnished in this condition by the organizational source and is the best copy available.

- This document may contain tone-on-tone or color graphs, charts and/or pictures, which have been reproduced in black and white.

- This document is paginated as submitted by the original source.

- Portions of this document are not fully legible due to the historical nature of some of the material. However, it is the best reproduction available from the original submission.

EVALUATION OF
THREE ANALYTICAL METHODS FOR STRUCTURES
UNDER RANDOM ACOUSTIC EXCITATION

FINAL REPORT

NORTHROP

EVALUATION OF
THREE ANALYTICAL METHODS FOR STRUCTURES
UNDER RANDOM ACOUSTIC EXCITATION

FINAL REPORT

NOR-71-102 August 1971

Prepared For
George C. Marshall Space Flight Center
National Aeronautics and Space Administration
Huntsville, Alabama

NASA CONTRACT NAS8-26195

(July 1970 — July 1971)

NORTHROP CORPORATION, AIRCRAFT DIVISION
3901 West Broadway
Hawthorne, California 90250

Chintsun Hwang, W. S. Pi (Authors)

CONTENTS

SUMMARY

The report describes an evaluation program on three analytical methods used in the response analysis of plate and shell structures under random acoustic excitation. The methods evaluated are (1) the statistical energy analysis (SEA) method, (2) the modal method, and (3) the Fourier transform method. In order to determine the applicability and the limitations of the methods, the basic assumptions and the formulations of these methods are reviewed. Additional analytical derivations are performed in order to explore the problems involved in the basic formulations of the analyses. Based on the analytical and the supporting experimental work, the workability and applicability of the methods are established. Some of the limitations and restrictions of the methods are postulated and described in detail.

SUMMARY

The report describes an evaluation program on three analytical methods used in the response analysis of plate and shell structures under random acoustic excitation. The methods evaluated are (1) the statistical energy analysis (SEA) method, (2) the modal method, and (3) the Fourier transform method. In order to determine the applicability and the limitations of the methods, the basic assumptions and the formulations of these methods are reviewed. Additional analytical derivations are performed in order to explore the problems involved in the basic formulations of the analyses. Based on the analytical and the supporting experimental work, the workability and applicability of the methods are established. Some of the limitations and restrictions of the methods are postulated and described in detail.

INTRODUCTION

The three methods evaluated in the subject program and described in the report are (1) the statistical energy analysis (SEA) method, (2) the modal method, and (3) the Fourier transform method. As is well known, these methods are different in origin and varied in their basic formulations. Their commonality lies in the fact that all methods have been applied in one way or another to predict the responses of plate and shell structures under random acoustic excitation. The purpose of the present investigation is to explore the assumptions and the analytical derivations of the methods in order to establish their applicability. Certain limitations and restrictions intrinsic to the methods are probed and illustrated. While the three diverse methods are evaluated consecutively, their merits and shortcomings, if any, are dealt with separately and independently. In general, it is expected that the information collected in the report will assist the prospective users to apply the analytical methods intelligently and selectively in solving practical problems.

The SEA method has its origin in room acoustics. The basic theory establishes the power flow between groups of uncoupled linear oscillators. Chronologically, a paper published by Lyon and Maidanik in 1962 (Reference 1) gives the detail theoretical foundation of the SEA and its application to a structure excited by a reverberant acoustic field. It also describes the equivalent electric circuits whose multimodal response is similar to that of a structure under random loadings. In 1962, Smith and Maidanik also published separate papers (References 2, 3), both of which deal with the responses of structural panels and their interaction with an acoustic field. In these papers, the level of excitation of the structure is formulated based on the radiation and mechanical resistances, as well as the spectral density of the pressure field. Since 1962, a number of papers and reports have appeared in literature (References 4-18), which postulate, extend, and apply the SEA to various problems involving randomly excited structures. Among them, a paper by Lyon and Eichler (Reference 4) describes the application of SEA to connected structures. Another paper by Crocker and Price (Reference 5) describes the successful application of SEA to sound transmission between partitioned rooms. Other papers related to the subject area are listed as References 19-30.

The second method being evaluated in the subject program is the modal method. The modal method has been used extensively to calculate the frequency responses of structures subjected to external excitation. The approach, which is applicable to either deterministic or random acoustic excitation, is based on the assumption that the responses may be represented in terms of an infinite number of natural modes of the structure (References 31-33). The formulation takes the form of either a single or double infinite series. In the series, each term represents the modal response (as a function of the frequency) which is determined by the modal force and the modal impedance. For practical structures, it is well known that the infinite series converges. The rate of convergence is dependent on the modal frequency distribution, the modal impedance, the acoustic input, etc. In order to truncate the infinite series for modal response computation in a rational manner, it is necessary to estimate the truncation error based on the modal data. The usefulness of the modal method for random response analysis is thus dependent on the ability to establish a reasonable limit of truncation error within the frequency range of interest when a finite number of natural modes is used.

The inherent limitation of the modal method lies in the fact that the modal density of a 2- or 3-dimensional continuous structure increases with frequency. With increasing frequency, proportionately more modes are needed in the response analysis, which in turn tax the capacity and accuracy requirements in the computation.

In the report, a method to calculate the truncation error for plate and shallow shell structures has been formulated. An error analysis is performed involving the estimates of series residues corresponding to various structural configurations. The basic scheme of the computation makes use of the wave number presentation which has been applied by Courant (Reference 34), Bolotin (References 35 and 36), Wilkinson (Reference 37), and others in structural modal density study. Using the approach, the truncation error of the modal method is established at the resonance frequencies of the structure as a function of the ratio of the resonance frequency versus the cutoff frequency.

The Fourier transform method is a highly developed technique which transforms a set of functional data from one domain to another by resolving the function into Fourier components. Through the transformation, certain advantages are gained which include: (1) ease of operations on the function such as integrations and differentiations, etc., (2) better insight in the nature and makeup of the function, and (3) adaptability to the numerical computation technique and/or the use of the Residue Theorem for the inverse transform. The Fourier transform technique has been used extensively in transient dynamic analysis and electric circuit analysis (Reference 38).

In transforming the structural displacement from the space domain to the wave number domain, the Fourier transform technique has been used in random vibration of structures (References 3, 40). In this type of application, it is desirable that the structure dimension be infinite or semi-infinite. For a finite structure such as a finite plate or shell panel, the application of the Fourier transform technique involves the introduction of line loads at the structure boundary (or boundaries) so that the boundary conditions may be satisfied. In this report, some exploratory work along this line is described.

The evaluation work covers the analytical methods developed by a number of research workers, many of whom are presently active in the field. During our investigation. we have corresponded with several authors whose papers appeared in the literature. These communications are acklowledged at appropriate locations of the report. The findings presented herewith represent the personal opinion of the authors of this report.

The authors wish to acknowledge the encouragement and support of Mr. Richard W. Schock and Dr. Hugo Steiner, both of the Aeronautics Laboratory of NASA Marshall Space Flight Center. Dr. Steiner served as the program monitor of the work reported herein. The experimental work described in this report was carried out by Mr. D.C. Skilling of Northrop.

EVALUATION OF THE STATISTICAL ENERGY ANALYSIS (SEA) METHOD

Our findings with respect to the SEA as applied to the plate and shell structures under random acoustic loading are listed below. The basis for and the reasoning behind our conclusions are described in the subsequent subsections.

1. SEA is based on an analysis of the energy transfer between linear oscillator systems with weak coupling. The theory is sound and may be applied to specific problems if all the basic assumptions are satisfied.

2. Based on available data, SEA is considered satisfactory in solving response problems involving interface(s) between a structure and a reverberant pressure field(s).

3. Based on the configurations investigated, the weak coupling conditions are generally not satisfied in problems dealing with connected solid structures. This is especially true in the low and medium frequency ranges where the modal response data of each substructure are noticeably affected by the substructure interface. We noted in a number of working examples in the literature illustrating SEA where the computations were extended to such frequencies that the basic assumptions could not be met. On the other hand, there is justification to apply SEA to structures under very high frequency excitation where (i) the wave patterns are diffused, (ii) the major wave lengths of interest are small compared with the characteristic dimension of the structure, and (iii) the displacement response patterns are almost independent of the structural boundaries and interfaces. In general, caution is suggested in applying SEA to fabricated aerospace structures.

4. The concept of establishing a probability function for the response data considering the variances of the energy based on analytical response functions is considered sound. In order to establish a confidence level in SEA prediction, a distribution function has to be assumed. The variances are usually computed based on (i) ideal and diffused modal patterns, and (ii) essentially linear responses of the oscillators with correction in the damping constants due to weak coupling. In reality, the variances in energy may be contributed

to factors not considered in the analysis. The above conditions make the establishment of a confidence level of the predicted data extremely difficult.

Assumptions of the SEA

The SEA is based on the power flow between groups of linear oscillators. Within each group (substructure), the modal data of the oscillators are governed by an eigen equation; no power flow is assumed to take place among the oscillators. Between two groups, the power flow is established by a set of dynamic equations. Each equation represents the mode response of one oscillator and its weak coupling with one or more oscillators from the other group. It is assumed that the weak couplings are such that the original eigenvectors may be retained in formulating the power flow. The coupling parameters are classified into inertia, damping, and spring types. For a stationary process, the assumption that the damping coupling parameters for any two oscillators are equal in magnitude and opposite in sign gives rise to a condition called gyroscopic coupling. Specifically, a gyroscopic coupling element is defined as one which produces a negative coupling force on oscillator (2) due to a positive velocity of oscillator (1) if it results in a positive force on oscillator (1) due to a positive velocity of oscillator (2) (Reference 11). The gyroscopic coupling causes the power flow coefficients to be equal in the two-way flows between the oscillators. As will be shown later, a substantial part of SEA involves the derivation of the power flow coefficient under the weak gyroscopic coupling condition.

Consider a narrow frequency band for which the modal density of the substructure may be determined either experimentally or analytically. In SEA, it is assumed that the input power spectrum is fairly flat within the frequency band. Each linear oscillator which is directly excited by the external source is considered to be subject to a "thermal bath." Under this condition, the modal energies of all the oscillators whose natural frequencies lie within the narrow band are fairly equal and may be represented by an average value. A final formulation of the SEA involves the response level of two or more substructures (which may be either connected substructures or a structure and a reverberant acoustic field) based on the average modal energies of the externally excited and the coupled oscillators.

General Formulation of the SEA

The formulation of the SEA described here follows the general scheme of Reference 1. We use double subscripts for the equivalent modal energies in order to

make their meaning more explicit. Additional equations are derived which relate the damping constant of the coupled substructure to the power flow coefficient between the oscillators. The result is used to evaluate the magnitude of the coupling parameter as well as the degree of coupling between oscillators based on available test data.

Consider two groups of multiple oscillators. Within each group (or substructure), the oscillators are uncoupled. Power flows take place between the oscillators of the two groups. The modal displacements of the oscillators are denoted by x_i, y_j respectively. Assuming weak gyroscopic coupling with only damping type terms, the following set of equations is established:

$$\begin{cases} \ddot{x}_i + \beta_i \dot{x}_i + \omega_i^2 x_i + \sum_{k=1}^{\bar{N}} B_{ik} \dot{y}_k = f_i & i = 1, \cdots, N \quad (1) \\ \ddot{y}_j + \bar{\beta}_j \dot{y}_j + \bar{\omega}_j^2 y_j - \sum_{\ell=1}^{N} B_{\ell j} \dot{x}_\ell = \bar{f}_j & j = 1, \cdots, \bar{N} \quad (2) \end{cases}$$

where β_i, β_j are the damping coefficients of the oscillators i, j; ω_i, $\bar{\omega}_j$ are the natural frequencies; B_{ik}, $B_{\ell j}$ are the coupling parameters ($B_{ik} = B_{ki}$, etc.); and f_i, $\bar{f}_j$ are the modal forces. Assuming a stationary process, the time average of a function is denoted by a pair of brackets $\langle\ \rangle$ around the function. The power balance equations may be expressed as follows:

$$\begin{cases} \beta_i \left\langle \dot{x}_i^2 \right\rangle = \beta_i \theta_i - \sum_{k=1}^{\bar{N}} g_{ik} (\theta'_{ik} - \bar{\theta}'_{ki}) & i = 1, \cdots, N \quad (3) \\ \bar{\beta}_j \left\langle \dot{y}_j^2 \right\rangle = \bar{\beta}_j \bar{\theta}_j + \sum_{\ell=1}^{N} g_{\ell j} (\theta'_{\ell j} - \bar{\theta}'_{j\ell}) & j = 1, \cdots, \bar{N} \quad (4) \end{cases}$$

or

$$\begin{cases} \beta_i \left\langle \dot{x}_i^2 \right\rangle = \beta_i \theta'_{ij} - g_{ij} (\theta'_{ij} - \bar{\theta}'_{ji}) & (5) \\ \bar{\beta}_j \left\langle \dot{y}_j^2 \right\rangle = \bar{\beta}_j \bar{\theta}'_{ji} + g_{ij} (\theta'_{ij} - \bar{\theta}'_{ji}) & (6) \end{cases}$$

$i = 1, \cdots, N;\ j = 1, \cdots, \bar{N}$

where θ'_{ij}, $\bar{\theta}'_{ji}$ are called the equivalent modal energies as defined below:

$$\theta'_{ij} = \theta_i - \sum_{k \neq j}^{\bar{N}} g_{ik} (\theta_{ik} - \bar{\theta}'_{ki}) / \beta_i \quad (7)$$

$$\bar{\theta}'_{ji} \quad \bar{\theta}_j + \sum_{\ell \neq i}^{N} g_{\ell j} \left(\theta'_{\ell j} - \bar{\theta}'_{j\ell}\right) / \bar{\beta}_j \tag{8}$$

and

$$\theta_i = \left\langle f_i \dot{x}_i \right\rangle / \beta_i \tag{9}$$

$$\bar{\theta}_j = \left\langle \bar{f}_j \dot{y}_j \right\rangle / \bar{\beta}_j \tag{10}$$

$$g_{ij} = B_{ij}^2 \left(\beta_i \bar{\omega}_j^2 + \bar{\beta}_j \omega_i^2\right) / \left[\left(\bar{\omega}_j^2 - \omega_i^2\right)^2 + \left(\beta_i + \bar{\beta}_j\right)\left(\beta_i \bar{\omega}_j^2 + \bar{\beta}_j \omega_i^2\right)\right] \tag{11}$$

$$|B_{ij}| \ll \beta_i, \ \bar{\beta}_j \tag{12}$$

Equation (12) defines the relative magnitudes of the coupling parameter and the modal damping coefficients which represent the weak coupling condition, a key condition on which SEA is based. For the purpose of examining the validity of the weak coupling condition, we developed the following formulations (equations 13-21) independently of previous SEA work.

Thus, the relation between B_{ij} and g_{ij} is as shown below:

$$B_{ij} \left\langle \dot{x}_i \ \dot{y}_j \right\rangle = g_{ij} \left(\theta'_{ij} - \bar{\theta}'_{ji}\right) \tag{13}$$

Equations (7), (8), and (13) are used for defining the energy terms. Based on this formulation, the power diagram for a typical oscillator (x_i) and the oscillator (y_j) is shown in Figure 1. Taking the summation of the terms of Equation (6) with respect to index "i" from 1 to N yields

$$N\bar{\beta}_j \left\langle \dot{y}_j^2 \right\rangle = \bar{\beta}_j \sum_{i=1}^{N} \theta'_{ji} + \sum_{i=1}^{N} \left(\theta'_{ij} - \bar{\theta}'_{ji}\right) g_{ij} \tag{14}$$

Insertion of equation (4) into equation (14) gives the following expression

$$\sum_{i}^{N}{}_{1} \quad \bar{\theta}'_{ji} \quad \bar{\theta}_j + (N-1) \left\langle \dot{y}_j^2 \right\rangle \tag{15}$$

In equations (14) and (15), the unknown $\bar{\theta}'_{ji}$ may be represented in terms of $\left\langle \dot{y}_j^2 \right\rangle$ and $\left\langle \dot{x}_i^2 \right\rangle$. This is accomplished by solving the simultaneous equations (5) and (6) based on the weak coupling assumption:

$$\begin{cases} \theta'_{ij} = (1 + \epsilon_i) \left\langle \dot{x}_i^2 \right\rangle - \epsilon_i (1 + \epsilon_i + \epsilon_j) \left\langle \dot{y}_j^2 \right\rangle & (16) \\ \bar{\theta}'_{ji} = (1 + \epsilon_j) \left\langle \dot{y}_j^2 \right\rangle - \epsilon_j (1 + \epsilon_i + \epsilon_j) \left\langle \dot{x}_i^2 \right\rangle & (17) \end{cases}$$

where $\epsilon_j = g_{ij} / \bar{\beta}_j$

$\epsilon_i = g_{ij} / \beta_i$

Insertion of equation (17) into equation (15) yields the relationship between $\left\langle \dot{y}_j^2 \right\rangle$ and $\left\langle \dot{x}_j^2 \right\rangle$:

$$\dot{y}_j^2 = \frac{\bar{\beta}_j \bar{\theta}_j - \sum_{i=1}^{N} g_{ij} \left\langle \dot{x}_i^2 \right\rangle}{\bar{\beta}_j + \sum_{i=1}^{N} g_{ij}} \qquad (18)$$

If there is no source on oscillator system y, equation (18) becomes:

$$\left\langle \dot{y}_j^2 \right\rangle = \left\langle \dot{\bar{x}}^2 \right\rangle \frac{\sum_{i=1}^{N} g_{ij}}{\bar{\beta}_j + \sum_{i=1}^{N} g_{ij}} \qquad (19)$$

where $\left\langle \dot{\bar{x}}^2 \right\rangle$ is a function proportional to the average energy contained in each individual oscillator of system x. Equation (19) may be rewritten for the multi-modal system where the average values of the modal energy, the damping coefficient, and the coupling damping factor are established for each group of oscillators within the frequency band $(\omega - 1/2\Delta\omega, \omega + 1/2\Delta\omega)$. Expressed in terms of functions related to the substructures, the final equation is:

$$\left\langle \dot{\bar{v}}^2 \right\rangle / \left\langle v^2 \right\rangle = \frac{M \bar{N}}{\bar{M} N} \frac{\beta_c}{\bar{\beta} + \beta_c} \qquad (20)$$

where the M, N, $\langle v^2 \rangle$ are the mass, the mode count, and the mean velocity square of the substructure excited externally; and $\bar{M}$, $\bar{N}$, $\langle \bar{v}^2 \rangle$ are the corresponding functions for the coupled substructure. $\bar{\beta}$ is the average modal damping coefficient of the coupled substructure and β_c is the coupling damping factor defined below :

$$\beta_c = \text{Mean of} \left(\sum_{i=1}^{N} g_{ij} \right) \quad \text{for all j's} \tag{21}$$

With the term β_c defined by equation (21), equation (20) conforms to the general formulation of the SEA (see equation 27, Reference 4).

SEA Applied to a Structure in a Reverberant Acoustic Field

Formulation of SEA as applied to a structure and a reverberant acoustic field may be found in Reference 1. Using basic equations of power flow, such as equations (3), (4) of the previous subsection, Lyon and Maidanik* defined the mechanical and radiation resistance R_{mech}, R_{rad} of the structure:

$$\sum_m \epsilon_m \langle \dot{s}'^2_m \rangle R_{mech} = \sum_m \langle \dot{s}^2_m \rangle R_{mech}$$

$$= M \sum_m \beta_m \langle \dot{s}^2_m \rangle \tag{22}$$

$$\sum_m \epsilon_m \langle \dot{s}'^2_m \rangle R_{rad} = M \sum_{m,r} g_{mr} (\theta'_m - \theta'_r) \tag{23}$$

In the above equations, $\langle \dot{s}'^2_m \rangle$ is the mean square modal velocity averaged over time, while $\langle \dot{s}^2_m \rangle$ is the mean square modal velocity averaged over time and space. M is the mass of the structure and m, r are the indices for the structure modes and the acoustic field modes respectively. In equation (3), we multiply the terms by M and move the coupling energy terms to the opposite side of the equation. Taking summation with respect to index i, the following is reached:

*The authors acknowledge the assistance of Dr.'s Lyon and Maidanik who confirmed certain typographical errors in Reference 1.

$$M \sum_{i}^{N} \beta_i \theta_i = M \sum_{i}^{N} \beta_i \left\langle x_i'^2 \right\rangle + M \sum_{i}^{N} \sum_{k}^{\bar{N}} g_{ik} \left(\theta'_{ik} - \bar{\theta}'_{ki} \right) \tag{24}$$

It is noted that the mechanical resistance, as given in equation (22), is identical to the first term on the RHS of (24). The radiation resistance, as given in equation (23), is identical to the second term on the RHS of (24). We note that each of the equivalent energy functions θ'_m of equation (23) is dependent on all of the modes $\dot{q}_r$ of the acoustic field, and each θ'_r is dependent on all of the modes $\dot{s}_m$ in the vibrating structure. This point was explained previously in equations (7) through (10).

Lyon and Maidanik applied the above equations to a structure interacting with a reverberant acoustic field. For this case, the modal density of the structure is substantially smaller than that of the acoustic field:

$$n_s(\omega) \ll n_r(\omega) \tag{25}$$

Based on (25), the following may be deduced relating the equivalent modal energy of the structure to the power flow due to weak acoustic coupling:

$$\beta_m \theta'_m \gg g_{rm} \left(\theta'_r - \theta'_m \right) \tag{26}$$

which is equation (9.24) of reference 1. This relation in turn yields $\left\langle \dot{s}_m^2 \right\rangle \simeq \theta'_m$. In other words, the modal energy and the equivalent modal energy of the structure may be used without distinction. Additional assumptions in this formulation are that the average modal damping coefficients β_s, β_R exist, and that the modal energies for each substructure are approximately equal within the frequency band of interest.

With the assumptions described above, a ratio may be established between the pressure spectrum and the acceleration spectrum when the structure alone is excited:

$$\frac{S_p(\omega)}{S_a(2)} = \frac{1}{2\pi^2 n_R(\omega)} \frac{\rho}{c} \frac{R_{rad}}{\beta_R} \tag{27}$$

and when the acoustic field is excited:

$$\frac{S_a(\omega)}{S_p(\omega)} = \frac{2\pi^2 n_s(\omega)}{M} \frac{c}{\rho} \mu(\omega) \tag{28}$$

where $$\mu(\omega) = \frac{R_{rad}}{R_{mech} + R_{rad}} = \frac{\frac{1}{N_s(\omega)} \sum_{r,m} g_{mr}}{\beta_s + \frac{1}{N_s(\omega)} \sum_{r,m} g_{mr}} \tag{29}$$

In the above, ρ is the air density and c is the speed of sound. In Reference 5, Crocker and Price applied equations (27) through (29) and some additional formulations to predict the sound transmission loss, the radiation resistance, and the vibration of a partition in separate chambers. Also applied in the analytical prediction is the formulation of the panel radiation resistance to half space as a function of the panel geometry and the frequency ratio (f/f_c) developed by Maidanik (Reference 3). The experimental phase of Crocker and Price studies involves the measurement of the radiation resistance, the total resistance, the coupling factor, the modal density, the transmission loss, and the vibration response of the aluminum panel located between two chambers. In general, the measured data correlate well with the data predicted by the SEA. For instance, the panel response relative to the mass law when one of the chambers is excited by a loudspeaker is plotted for 1/3-octave in Figure 2, which is reproduced from Reference 5. The analytical data are overplotted as a continuous curve based on the following:

$$\frac{S_a(\omega)}{S_{a_{m\ell}}(\omega)} = \frac{\pi^2 f_c \rho_s}{2\rho_c} \frac{\eta_{rad}}{\eta_{int} + \eta_{rad}} \tag{30}$$

where

$$S_{a_{m\ell}} = \frac{2}{\rho_s^2} S_p(\omega) \tag{31}$$

In Figure 2, the agreement in theory and experiment is considered satisfactory. In the low-frequency range (<400 Hz), moderate disagreement is observed. It is worthy of mention that Crocker and Price attributed the cause of the discrepancy to the insufficiency of panel modes in the low-frequency range. The low modal density of the panel and the resulting spread of the panel/room interaction modes make a correct averaging process impossible, a factor not considered in the SEA.

In conclusion, the general success of the SEA, as applied to a structure interacting with a reverberant acoustic field(s), is believed due to the following:

1. Weak coupling exists between the panel and the acoustic field.

2. The weak coupling and the difference in modal densities of the panel and the acoustic chamber justify the use of the modal energy $\langle \dot{s}_m^2 \rangle$ and the equivalent modal energy, θ'_m, without distinction.

3. A valid formulation exists for the radiation resistance of a panel which makes possible the analytical determination of $\sum_{r,m} g_{mr}$. This formulation is carried in the wave number domain through the assumption of a completely diffused wave field.

The Extent of Coupling Between Substructures

In the basic formulation of the SEA, Equations (1- 12), it is assumed that the coupling is weak between any two oscillators of two substructures. This condition is represented by:

$$\left|B_{ij}\right| \ll \beta_i . \bar{\beta}_j \tag{12}$$

In this subsection, we attempt to establish an analytical relation between B, the root mean square value of B_{ij}, and the couple damping factor $\beta_c = \eta_c \omega_o$ for various center frequencies ω_o (η_c is denoted by η_{ss}^s in Reference 4). Since the couple damping factor β_c may be determined either analytically or experimentally for any given set of substructures, and since the average modal damping coefficient $\bar{\beta}$ (see equation 20) is usually determined experimentally, the analytical relation between $B^2 = \langle B_{ij}^2 \rangle$ and β_c developed here may be applied to check the validity of the weak coupling condition of (12).

As shown in equation (11) previously, g_{ij} may be expressed in terms of the coupling parameter B_{ij}, the natural frequencies of the oscillators, and the modal damping coefficients. Furthermore, the mean value of any function in group i is indicated by subscript 2 and the mean value of any function in group j is indicated by subscript 1. Based on this convention, the following is reached through the application of equation (21).

$$\beta_c(\omega_o) = B^2 \sum_{i=1}^{N} \frac{\beta_2 \omega_1^2 + \beta_1 \omega_i^2}{\left(\omega_i^2 - \omega_1^2\right)^2 + (\beta_1 + \beta_2)\left(\beta_2 \omega_1^2 + \beta_1 \omega_i^2\right)} \Bigg|_{\omega_1 - \frac{1}{2}\Delta\omega \le \omega_i \le \omega_1 + \frac{1}{2}\Delta\omega}$$

$$\simeq B^2 n_2 \int_{\omega_1 - \frac{1}{2}\Delta\omega}^{\omega_1 + \frac{1}{2}\Delta\omega} \frac{\left(\beta_2\omega_1^2 + \beta_1\omega^2\right) d\omega}{\left(\omega_1^2 - \omega^2\right)^2 + (\beta_1 + \beta_2)\left(\beta_2\omega_1^2 + \beta_1\omega^2\right)}$$

$$\simeq B^2 n_2 \int_{-\frac{1}{2}\Delta\omega}^{\frac{1}{2}\Delta\omega} \frac{(\beta_1 + \beta_2)\, d(\omega - \omega_1)}{4(\omega - \omega_1)^2 + (\beta_1 + \beta_2)^2}$$

$$\simeq B^2 n_2 \tan^{-1}\left(\frac{\Delta\omega}{\beta_1 + \beta_2}\right) \tag{32}$$

where $\omega_o = \omega_1$ = the center frequency

$\Delta\omega$ = frequency band width

n_2 = the modal density of substructure 2

$\beta_1 \quad \eta_1\omega_o$ = damping coefficient of substructure 1

$\beta_2 \quad \eta_2\omega_o$ = damping coefficient of substructure 2.

As mentioned previously, the term β_c appears in equation (20). Corresponding to equation (32), substructure (2) refers to the one which is excited externally, while substructure (1) refers to the coupled substructure. The damping coefficient $\bar{\beta}$ in equation (20) is thus equal to β_1 as shown in the equation above. When 1/3-octave frequency band width is used, equation (32) may be simplified to:

$$B^2 \simeq 2\beta_c(\omega_o)/n_2\pi = \left(2\eta_{ss}^s/n_2\pi\right)\omega_o \tag{33}$$

Based on the above equation, the values of B^2 may be computed as a function of n_2, ω_o and η_{ss}^s ($= \beta_c/\omega_o$). The application of the above equations is presented in the following subsection.

SEA Applied to Connected Structures

Since its introduction in 1962, substantial effort has been directed to the application of the SEA to connected structures such as fabricated aerospace structures. For this purpose, it is expected that the basic assumptions and conditions set up in the analysis are valid so that the response equation (equation 20) may be used for each frequency band. Furthermore, efforts have been made to determine the coupling loss

factor analytically and experimentally in order to apply the method for prediction purposes, corresponding to various structural configurations.

In Reference 4, Lyon and Eichler applied the SEA to the random vibration of connected structures. Two examples are covered in the paper, namely, a beam bonded to a corner-supported rectangular plate, and a vertical plate welded at right angles to a corner-supported rectangular plate (Figure 3 of this report). For the latter configuration, an edge absorption coefficient γ_{ij} is determined based on the flexural wave propagation equations in plates and the continuity conditions at the fabrication line of two plates i, j.

Specifically, γ is the ratio of the outgoing wave energy rate per unit length of the junction line vs the incoming wave energy rate in the other plate. The details of derivation of γ are presented in Reference 4.* Two cases of γ of special interest to the present program are described below:

(i) $h_1 = h_2$, $D_1 = D_2$,

$$\gamma_{12} = \frac{2}{9} \tag{34}$$

(ii) $h_1 \ll h_2$, $k_1 \gg k_2$

$$\gamma_{12} \cong \frac{1}{2} \left(h_1/h_2\right)^3 \tag{35}$$

For a structure made of two connected plates of specific dimensions, the coupling loss factor is given by Heckl (Reference 27) as:

$$\eta_c = \eta^s_{ss} = \frac{2}{\pi} \left(\frac{L}{k_1 A_1}\right) \gamma \tag{36}$$

where L is the length of the junction line and A_1 is the area of the plate which is excited externally.

In Reference 4, the loss factor $\eta_1 = \bar{\beta}/\omega_o$ is measured for plate no. 1 (the vertical web in Figure 3) before assembly. After assembly, the plate is excited impulsively at a random location on plate no. 1, and the combined loss factor $\eta_1 + \eta^s_{ss} \quad (\bar{\beta} + \beta_c)/\omega_o$ is determined based on the decay time measured at random locations of the same plate.

*In private communication, certain modification and additional derivation of γ were relayed to the authors by Dr. Eichler. These data are not covered in this report.

The loss factor data are used in equation (20) to predict the ratio of responses of the two plates when plate no. 2 is excited. This technique is based on the assumption that the power flow at the interface stops immediately after the impulsive load is released irrespective of to which substructure the load was applied. In Reference 4, η_1 and $\eta_1 + \eta^s_{ss}$ data are plotted as functions of the 1/3-octave frequency. Also plotted is the theoretical γ based on equation (35) and the γ data based on experimental η^s_{ss} and equation (36). The plot is duplicated in the present report as Figure 4.

An alternative form of equation (33) is used to define B, or the root mean square value of B_{ij}, where B_{ij} is the damping coupling parameter between an oscillator in substructure 2 (the base plate) and an oscillator in substructure 1 (the vertical web):

$$B = \left\langle B_{ij}^2 \right\rangle^{\frac{1}{2}} = \left(\frac{2 \eta^s_{ss} \omega_o}{n_2 \pi} \right)^{\frac{1}{2}} \tag{37}$$

This equation is used together with equation (36) to determine the ratio (B/β_1) at 1/3-octave frequency increments. The results are plotted in Figure 5. In the figure, the curve marked with dots is based on measured η^s_{ss} of the two-plate system (Figure 4). The curve marked with circles is based on the γ_{th} value of Equation (35) for the same two-plate system. For a different two-plate system where $h_1 = h_2 = .057"$, γ is determined by Equation (34). For this case, the (B/β_1) ratio is plotted as the curve marked with crosses in Figure 5. In examining these curves, it is obvious that the basic weak coupling condition (12), $|B_{ij}| \ll \beta_i, \beta_j$, is not satisfied at almost all frequencies. For $f < 7000$ Hz, the computed (B/β_1) values are greater than unity. The highest value is 11.4. Since equations (32, 33) are derived based on the weak coupling condition, the above data do not serve a positive proof as to the applicability or inapplicability of the SEA to the two-plate system. On the other hand, the extraordinarily high ratio of (B/β_1) suggests that substantial coupling exists between the connected plates. This observation casts doubt on the validity of the predicted responses based on the SEA. Additional experimental observations on the same connected structure are described subsequently.

Experiments on the Two-Plate System

A structure identical to the two-plate configuration described in Reference 4 and illustrated in Figure 3 of this report was fabricated and tested. Preliminary damping

tests were performed on the structure prior to the response tests. In the response tests, a shaker with sinusoidal and 1/3-octave frequency band inputs was used to supply the excitation force at various locations of the base plate. Fine polyvinyl chloride pellets were spread over the base plate to visualize the deflection pattern of the plate. The basic instrumentation system of the tests is shown schematically in Figure 6.

In the 1/3-octave response tests, the average response ratio of the two connected plates is acquired through a number of accelerometer readings. The data are plotted in Figure 7 in terms of 10 log $\left(v_1^2/v_2^2\right)$ for two locations of excitation. Similar data obtained in Reference 4 are also plotted in the same figure. Referring to the figure, the three sets of data correlate fairly well for frequencies above 4000 Hz. Below 4000 Hz, substantial deviations are observed between Lyon and Eichler data and our data. The discrepancy is believed due to minor differences in the method of fabrication and the supporting conditions for which the low-frequency modes are sensitive. The fairly consistent response data in the high-frequency region is partially contributed to the more diffused wave patterns in the plates.

The modal density of a plate is given in Reference (34) as:

$$n_p(f) = \sqrt{3}\, A_p/C_p t_p \tag{38}$$

where A_p is the area of the plate, t_p is the plate thickness, and C_p is the longitudinal wave speed of the plate material. Equation (38) gives $n_p(f) = .129$ modes/Hz for the base plate so that we are dealing with more than 115 modes in the 1/3-octave band at 4000 Hz center frequency. Our experiments show that under sinusoidal excitation, a clear deformation pattern exists which represents a superposition of a number of strong modes (Figure 8). This selection of the prominent modes is believed to be dictated by the boundary conditions, including the substructure interface. A 1/3-octave excitation yields a recognizable deformation pattern which resembles to a certain degree the pattern of the sinusoidal excitation (Figure 9).

At lower frequencies, features similar to those described above are observed when the plate is subject to the 1/3-octave and sinusoidal excitations. For 1/3-octave excitation, the wave pattern tends to break into smaller grids than those of the sinusoidal excitation, which suggests a higher degree in the superposition of modes, as it should be. In either case, the effects of the interface of the vertical plate to its deformation patterns are pronounced. Figures 10 and 11 are the visualized patterns

of sinusoidal and 1/3-octave excitations at 2000 Hz. We were able to obtain a fairly clear deformation pattern with 5000 Hz sinusoidal excitation and a much diffused pattern with 1/3-octave excitation. Above 5000 Hz, no clear pattern was recognizable when we used the pellet visualization technique.

It is worthy of mentioning that because of the usual spectral makeup of the acoustic loads and the high damping constant at very high frequencies, significant responses of the typical aerospace structure usually appear in the low and moderate frequency region. (See, for instance, Figures 9 and 10, Reference 28.) In view of the spectral distribution of the major responses in aerospace structures, and to the uncertainty regarding the applicability of the weak coupling condition of the connected substructures at moderate frequencies, it is considered advisable to perform certain preliminary investigations prior to the application of SEA. In the preliminary investigation the extent of coupling of the substructures, the degree of dependence of the mode shapes on the structure interface(s), and the natural constraints should be carefully evaluated. The preliminary data may then be used to determine the applicability and limitations of SEA.

EVALUATION OF THE MODAL METHOD

The modal method, as applied to random acoustic excitation of structures, is based on the assumption that the responses may be represented in terms of the infinite number of natural modes of the structure (References 31, 32, and 33). The formulation takes the form of either single or double infinite series. In the series, each term represents the modal response (as a function of frequency) which is determined by the modal force and the modal impedance. For practical structures, it is well known that the infinite series converges. The rate of convergency is dependent on the modal frequency distribution, the modal impedance, the frequency range of interest, etc. The convergence of the series justifies its truncation during computation. In order to truncate the infinite series for modal response computation in a rational manner, it is necessary to estimate the truncation error based on the modal data. In this section, a method is described to calculate the truncation error for plate and shallow shell structures under specified random loads. Similarly, when the finite element approach is used, the responses of the structure at selected locations are presented in terms of the modal matrices. Since the number of modes used is equal to the matrix column number, the matrix presentation implies a modal truncation.

The modal method is most suitable in determining the responses in the low-frequency region. The upper limit of operation of the method is influenced by the following factors:

1. When the finite element approach is employed, the number of modes used in the modal analysis is restricted by:
   a. The amount of the structural details available in the analysis
   b. The capacity and accuracy of the eigenvalue routine
   c. The computer capacity and processing time requirement.
2. The modal truncation limits the application of the modal method only to the frequency range where the natural modes are properly covered.
3. Corresponding to the highest frequency natural mode, the modal pattern has a characteristic wave number, i.e., a typical wave length. When the finite

element method is applied, this wavelength has to be a multiple of the typical length between two neighboring reference joints in order that sufficient accuracy may be retained in both the eigen vectors and the eigen frequencies. This condition limits the application of the modal method up to a certain wave number.

Modal Method Formulation Using the Finite Element Method

In the matrix formulation, the equation of motion of a damped elastic structure is:

$$[M]\{\ddot{w}\} + [C]\{\dot{w}\} + [K]\{w\} = \{f(t)\} \tag{39}$$

where w is the matrix of nodal point deflection components, M is the mass matrix, C is the damping matrix, K is the stiffness matrix of the structure, and f(t) is the matrix of external nodal point forces.

In the modal analysis, the nodal displacements w are approximated by the finite series of the eigen vectors in the following matrix form:

$$\{w\} = [Q]\{\xi(t)\} \tag{40}$$

where Q is a rectangular matrix whose columns are the eigen vectors. The analysis satisfies the following orthogonality conditions:

$$[Q]^T [M] [Q] = \lceil I \rfloor \tag{41}$$

$$[Q]^T [K] [Q] = \lceil \bar{\omega}^2 \rfloor \tag{42}$$

where $\bar{\omega}_i$ represents the eigen frequency of the i-th eigen vector. In order to simplify the problem, the generalized damping matrix is usually assumed to be a diagonal matrix:

$$[Q]^T [C] [Q] = 2 \lceil \gamma \rfloor \lceil \bar{\omega} \rfloor \tag{43}$$

where γ_i represents the damping ratio of the i-th mode.

The insertion of equations (40) - (43) into equation (39) leads to the matrix equation for the generalized coordinate $\xi(t)$:

$$\{\ddot{\xi}\} + 2 \lceil \gamma \rfloor \lceil \bar{\omega} \rfloor \{\dot{\xi}\} + \lceil \bar{\omega}^2 \rfloor \{\xi\} = [Q]^T \{f(t)\} \tag{44}$$

In the frequency domain, the Fourier transform of w may be simply expressed in terms of the Fourier transform of external forces as:

$$\{S_w(\omega)\} = [Q]\{S_\xi(\omega)\} = [Q]\lceil H(\omega)\rfloor[Q]^T\{S_f(\omega)\} \tag{45}$$

The j-th element of the diagonal admittance matrix H (ω) is defined as

$$H_j(\omega) = 1/\left[\omega_j^2 - \omega^2 + 2i\omega\omega_j\gamma_j\right] \tag{46}$$

Furthermore, the structure response PSD for random loading may be computed based on the matrices described above:

$$[\phi_w(\omega)] = [Q]\lceil H(\omega)\rfloor[Q]^T[\phi_f(\omega)][Q]\lceil H^*(\omega)\rfloor[Q]^T \tag{47}$$

The asterisk above a matrix indicates the complex conjugate of the matrix. The diagonal elements of the matrices ϕ represent the PSD values, while the off-diagonal terms represent the cross-PSD values.

With matrix $\phi_w(\omega)$ determined, the mean-square values of deflections may be obtained by integrating the corresponding diagonal elements of ϕ_w numerically.

Truncation Error In Modal Analysis

In the following, a method is established to compute the truncation error in the modal analysis of a plate or double-curved panel under random acoustic excitation. The panel modal response is represented by an infinite series. In evaluating the spectral response data, the error introduced due to the truncation of the infinite series is computed based on the wave number presentation. Using this approach, the truncation error of the modal method is established at the resonance frequencies of the panel as a function of the ratio of the resonance frequency versus the cutoff frequency. Various types of the input acoustic spectra may be applied in the process. For illustration purpose, error analyses are performed on a simply supported plate and a shallow spherical shell subjected to uniform intensity random loads.

In the modal formulation, the power spectrum density (PSD) of deflection at location i may be expressed in the following form (also see equation (47)):

$$\phi_{w_{ii}}(\omega, \omega_N) = \sum_{j=1}^{N}\sum_{\ell=1}^{N} Q_{ij}\,Q_{i\ell}\,\mathrm{Re}\left[\phi_{F_{j\ell}}(\omega)\,H_j(\omega)\,H^*_\ell(\omega)\right]\Big|_{\bar\omega_j,\,\bar\omega_\ell \le \omega_N} \tag{48}$$

where

ω = frequency in rad/sec

ω_N = cutoff frequency, i.e., upper bound of natural frequencies in modal truncation

$\Phi_{F_{jl}}(\omega)$ = cross PSD of modal forces F_j and F_l

At the resonance frequencies $\bar{\omega}_p$ (p = 1, 2, . . . N) of the structure, the response PSD has the following approximate peak values:

$$\Phi_{w_{ii}}(\bar{\omega}_p, \omega_N) \cong Q_{ip}^2 \left(4\gamma_p^2 \bar{\omega}_p^4\right)^{-1} \Phi_{F_{pp}}(\bar{\omega}_p) + Q_{ip}\left(\gamma_p \bar{\omega}_p^2\right)^{-1} \sum_{\substack{l=1 \\ l \neq p}}^{N} Q_{il}\, \mathrm{Im}\left[\Phi_{F_{pl}}(\bar{\omega}_p)\, H_l^*(\bar{\omega}_p)\right]$$
$$+ \sum_{\substack{l=1 \\ l \neq p}}^{N} Q_{il}^2\, \Phi_{F_{ll}}(\bar{\omega}_p) \left|H_l(\bar{\omega}_p)\right|^2 \tag{49}$$

where

$\bar{\omega}_p, \bar{\omega}_l \leq \omega_N$.

The error of the response PSD due to modal truncation is:

$$\Delta\Phi_{w_{ii}}(\bar{\omega}_p, \omega_N) \cong Q_{ip}\left(\gamma_p \bar{\omega}_p^2\right)^{-1} \sum_{l=N+1}^{\infty} Q_{il}\, \mathrm{Im}\left[\Phi_{F_{pl}}(\bar{\omega}_p)\, H_l^*(\bar{\omega}_p)\right]$$
$$+ \sum_{l=N+1}^{\infty} Q_{il}^2\, \Phi_{F_{ll}}(\bar{\omega}_p) \left|H_l(\bar{\omega}_p)\right|^2 \tag{50}$$

The relative error due to truncation is simply:

$$\epsilon = \Delta\Phi_{w_{ii}}(\bar{\omega}_p, \omega_N) / \Phi_{w_{ii}}(\bar{\omega}_p, \omega_N) \tag{51}$$

Truncation Errors For Double Curved Panels

In general, the asymptotic expression of the natural frequencies $\bar{\omega}$ may be used for the modes of vibration having sufficiently large wave numbers. For a rectangular

elastic shell element whose orthogonal curvilinear coordinates x and y coincide with the lines of principal curvatures, the asymptotic frequency equation is (Reference 35):

$$\bar{\omega}^2 = \frac{D}{\rho h}\left[\left(k_1^2 + k_2^2\right)^2 + \frac{Eh}{D}\frac{\left(\frac{k_1^2}{R_2} + \frac{k_2^2}{R_1}\right)^2}{\left(k_1^2 + k_2^2\right)^2}\right] \tag{52}$$

where R_1 and R_2 are the radii of curvature of the middle surface, E the Young's modulus, ρ the density of the material, D the plate stiffness, h the thickness, and k_1, k_2 the wave numbers. It has been shown by Bolotin (Reference 41) that in the absence of a dynamic edge effect in which the boundary conditions have a considerable effect on the mode shapes in the interior of the shell, the wave numbers of shallow shells can be approximated by

$$\begin{aligned} k_1 &= m\pi/a + 0(1), \qquad m = 1, 2, \ldots \\ k_2 &= n\pi/b + 0(1), \qquad n = 1, 2, \ldots \end{aligned} \tag{53}$$

where a and b are the edge lengths. The term 0(1) represents a term of the order of unity. It is expected that corresponding to the cut-off frequency of the shallow shell, either k_1 or k_2, or both, are of an order of magnitude much greater than unity. If the boundary is simply supported, the asymptotic solution coincides with the exact one and the wave numbers k_1 and k_2 are given as:

$$k_1 = m\pi/a, \qquad k_2 = n\pi/b \tag{54}$$

Following the same reasoning, it is noted that $M(\omega_{N_1}, \omega_{N_2})$, the total number of modes whose natural frequencies are within the frequency band $(\omega_{N_1}, \omega_{N_2})$, may be determined approximately on the (k_1, k_2) plane. Specifically, area integration is carried out in the first quadrant of the plane which is bounded by the k_1, k_2 axes and the two curves defining $\omega = \omega_{N_1}$ and $\omega = \omega_{N_2}$. The equation for M is given below:

$$M\left(\omega_{N_1}, \omega_{N_2}\right) = \frac{1}{\Delta k_1 \, \Delta k_2} \iint_S dk_1 \, dk_2 \tag{55}$$

where $\Delta k_1 = \pi/a$ and $\Delta k_2 = \pi/b$. Applying the transformation

$$\begin{aligned} k_1 &= r \cos\theta \\ k_2 &= r \sin\theta \end{aligned} \tag{56}$$

the following is reached:

$$M\left(\omega_{N_1}, \omega_{N_2}\right) \simeq \frac{ab}{\pi^2} \iint_S r \, dr \, d\theta \tag{57}$$

Similarly, the error of the response PSD due to modal truncation may be derived based on equations (46), (50), (52), (56), and (57):

$$\begin{aligned} \Delta\phi_{w_{ii}}(\bar{\omega}_p, \omega_N) \cong & \sum_{\ell=N+1}^{\infty} \frac{Q_{i\ell}}{\left[\left(\bar{\omega}_\ell^2 - \bar{\omega}_p^2\right)^2 + 4\gamma_\ell^2 \bar{\omega}_\ell^2 \bar{\omega}_p^2\right]} \left\{ Q_{i\ell} \phi_{F_{\ell}}(\bar{\omega}_p) \right. \\ & \left. + \frac{Q_{ip}}{\gamma_p \bar{\omega}_p^2} \left[2\gamma_\ell \bar{\omega}_p \bar{\omega}_\ell \, \mathrm{Re}\left[\phi_{F_{p\ell}}(\bar{\omega}_p)\right] + \left(\bar{\omega}_\ell^2 - \bar{\omega}_p^2\right) \mathrm{Im}\left[\phi_{F_{p\ell}}(\bar{\omega}_p)\right] \right] \right\} \\ \cong & \frac{ab}{\pi^2} \int_{\theta_1}^{\theta_2} \int_{r(\omega_N)}^{\infty} \frac{\left(\frac{\rho h}{D}\right)^2 Q_{i\ell}}{\left[\left(r^4 + \frac{\rho h}{D}\alpha - \bar{k}_p^4\right)^2 + 4\gamma_\ell^2 \bar{k}_p^4 \left(r^4 + \frac{\rho h}{D}\alpha\right)\right]} \left\{ Q_{i\ell} \phi_{F_{\ell\ell}}(\bar{\omega}_p) \right. \\ & + \frac{Q_{ip}}{\gamma_p \bar{k}_p^4} \left[2\gamma_\ell \bar{k}_p^2 \left[r^4 + \frac{\rho h}{D}\alpha\right]^{1/2} \mathrm{Re}\left[\phi_{F_{p\ell}}(\bar{\omega}_p)\right] \right. \\ & \left. \left. \left. + \left(r^4 + \frac{\rho h}{D}\alpha - \bar{k}_p^4\right) \mathrm{Im}\left[\phi_{F_{p\ell}}(\bar{\omega}_p)\right] \right] \right\} r \, dr \, d\theta \end{aligned} \tag{58}$$

where

$$\bar{\omega}_\ell = \left[\frac{D}{\rho h} r^4 + \alpha(\theta)\right]^{1/2} \tag{59}$$

$$\alpha(\theta) = \frac{E}{\rho}\left(\frac{\cos^2\theta}{R_2} + \frac{\sin^2\theta}{R_1}\right)^2 \tag{60}$$

$$\bar{\omega}_p = (D/\rho h)^{1/2} \bar{k}_p^2 \tag{61}$$

$$\bar{k}_p^2 \quad \left[\left(k_{1p}^2 \quad k_{2p}^2 \right)^2 + \frac{Eh}{D} \frac{\left(\frac{k_{1p}^2}{R_2} + \frac{k_{2p}^2}{R_1} \right)^2}{\left(k_{1p}^2 + k_{2p}^2 \right)^2} \right]^{1/2} \tag{62}$$

$$r(\omega_N) \quad \left\{ (\rho h/D) \left| \omega_N^2 - \alpha(\theta) \right| \right\}^{1/4} \tag{63}$$

The integration is carried out over the first quadrant of the (k_1, k_2) plane, the details of which are described in the subsequent sections.

Random Pressure Loads

Consider the case of a simply supported shallow shell element with double curvatures under uniform intensity random loads $\phi_o(\omega)$ $(psi)^2/Hz$. The random loads are spatially deterministic, i.e., they are in perfect spatial correlation.

The ℓ-th mode shape at location i (x, y) of the shell element is:

$$Q_{i\ell} = A \sin k_{1\ell} x \sin k_{2\ell} y \tag{64}$$

where

$$A \quad 2(\rho h ab)^{-1/2}, \quad k_{1\ell} = \ell_1 \pi/a, \quad k_{2\ell} = \ell_2 \pi/b. \tag{65}$$

The corresponding natural frequency is given by equation (52). The cross-PSD of the modal forces F_ℓ and F_m is:

$$\phi_{F_{\ell m}}(\omega) \quad 16 \ \phi_o(\omega) A^2 \left(k_{1\ell} k_{2\ell} k_{1m} k_{2m} \right)^{-1} \tag{66}$$

where $k_{1\ell} = \frac{\ell_1 \pi}{a}$, etc., ℓ_1, ℓ_2, m_1, m_2 = odd integers. (67)

Based on equation (58), the truncation error of the center deflection PSD of the element may be expressed as:

$$\Delta\phi_W(\bar{\omega}_p, \omega_N) \simeq 4 \phi_o(\bar{\omega}_p) A^4 \left(\frac{\rho h}{D} \right)^2 \left(\frac{2}{ab} \right) \left(k_{1p} k_{2p} \bar{k}_p^2 \right)^{-1}$$

$$\int_{\theta_1}^{\theta_2} \int_{r_o(\theta)}^{\infty} \frac{k_{1p} k_{2p} \bar{k}_p^2 + 2 r^2 \cos\theta \sin\theta \left(r^4 + \frac{\rho h}{D} \alpha \right)^{1/2}}{\left(r^4 + \frac{\rho h}{D} \alpha - \bar{k}_p^4 \right)^2 r^4 \cos^2\theta \sin^2\theta} r \, dr \, d\theta \tag{68}$$

In equation (68), the factor in the denominator of the integrand

$$\left[\left(r^4 + \frac{\rho h}{D}\alpha - \bar{k}_p^4\right)^2 + 4\gamma_\ell \bar{k}_p^4 \left(r^4 + \frac{\rho h}{D}\alpha\right)\right]$$

has been replaced by $\left(r^4 + \frac{\rho h}{D}\alpha - \bar{k}_p^4\right)^2$ approximately since $\gamma_\ell \ll 1$ and $\bar{\omega}_\ell > \bar{\omega}_p$. The approximation tends to make the computed truncation error on the conservative side since the impedance magnitude is reduced. Furthermore, the value of $\Delta k_1 \Delta k_2 \quad ab/\pi^2$ has been replaced by $ab/(4\pi^2)$. This is because only the odd wave numbers contribute to the response.

Figure 12 shows the modal distribution of the element in the wave number domain. The double integrals are carried out over the shaded area in Figure 12(a).

It is noted that the narrow strips next to the k_1, k_2 axes are excluded from the area of integration. The exclusion, which forestalls the divergence of the integrand of equation (68), is justifiable because no natural frequencies exist in these strips.

The boundary of the area of integration is defined by the following:

$$\begin{array}{lllll} \overline{AB}: & 0 \le \theta \le \beta_1 & r_o(\theta) & \pi/(b \sin\theta) \\ \overset{\frown}{BC}: & \beta_1 \le \theta \le \beta_2 & r_o(\theta) & r(\omega_N) \\ \overline{CD}: & \beta_2 \le \theta \le \frac{\pi}{2} & r_o(\theta) & \pi/(a \cos\theta) \end{array} \qquad (69)$$

The angles β_1 and β_2 are determined by the equations which follow:

$$\sin\beta_1 = \frac{\pi}{b\, r_o(\beta_1)} = \frac{\pi}{b}\left\{\frac{\rho h}{D}\left[\omega_N^2 - \frac{E}{\rho}\left(\frac{\cos^2\beta_1}{R_2} + \frac{\sin^2\beta_1}{R_1}\right)^2\right]\right\}^{-1/4}$$

$$\cos\beta_2 = \frac{\pi}{a\, r_o(\beta_2)} = \frac{\pi}{a}\left\{\frac{\rho h}{D}\left[\omega_N^2 - \frac{E}{\rho}\left(\frac{\cos^2\beta_2}{R_2} + \frac{\sin^2\beta_2}{R_1}\right)^2\right]\right\}^{-1/4} \qquad (70)$$

From equations (68) through (70), it is noted that the integration over the areas $0 \le \theta \le \beta_1$ and $\beta_2 \le \theta \le \frac{\pi}{2}$ will yield very complicated expressions for θ. In order to simplify the problem, only the shaded area shown in Figure 12(b) is integrated, i.e., $r_o(\theta) = r(\omega_N)$, $\beta_1 \le \theta \le \beta_2$. Since β_1 and $\frac{\pi}{2} - \beta_2$ are small quantities in comparison

with $\frac{\pi}{2}$ when ω_N is sufficiently large, the approximation is considered acceptable. With this simplification, the integral in equation (68) may be carried out with respect to r as shown below:

$$\Delta\phi_W(\bar{\omega}_p, \omega_N) \cong 2\,\phi_o(\bar{\omega}_p)\,A^4\left(\frac{ab}{\pi^2}\right)\left(k_{1p}\,k_{2p}\,\bar{\omega}_p\right)^{-1}$$

$$\int_{\theta_1}^{\theta_2} \frac{\left(\frac{D}{\rho h}\right)^{1/2} k_{1p}\,k_{2p}\,\bar{\omega}_p}{\left[\bar{\omega}_p^2 - \alpha(\theta)\right]^2 \cos^2\theta\,\sin^2\theta}\left[\frac{1}{\left[\Omega^2 - \alpha(\theta)\right]^{1/2}} + \frac{\left|\Omega^2 - \alpha(\theta)\right|^{1/2}}{2\left(\Omega^2 - \bar{\omega}_p^2\right)}\right.$$

$$+ \frac{3}{4\left[\bar{\omega}_p^2 - \alpha(\theta)\right]^{1/2}}\,\ell n\,\frac{\left|\bar{\omega}_p^2 - \alpha(\theta)\right|^{1/2}\left[\Omega^2 - \alpha(\theta)\right]^{1/2} - \bar{\omega}_p^2 + \alpha(\theta)}{\left|\bar{\omega}_p^2 - \alpha(\theta)\right|^{1/2}\left|\Omega^2 - \alpha(\theta)\right|^{1/2} + \bar{\omega}_p^2 - \alpha(\theta)}\Bigg]$$

$$+ \frac{1}{\left[\bar{\omega}_p^2 - \alpha(\theta)\right]^2 \cos\theta\,\sin\theta}\left[\frac{\Omega\left[\bar{\omega}_p^2 - \alpha(\theta)\right]}{\Omega^2 - \bar{\omega}_p^2} - \alpha^{1/2}(\theta)\,\ell n\,\frac{\Omega - \alpha^{1/2}(\theta)}{\Omega + \alpha^{1/2}(\theta)}\right.$$

$$\left.\left. + \frac{\bar{\omega}_p^2 + \alpha(\theta)}{2\bar{\omega}_p}\,\ell n\,\frac{\Omega - \bar{\omega}_p}{\Omega + \bar{\omega}_p}\right]\right\}\Bigg|_{\Omega = \left[\frac{D}{\rho h}\,r^4(\omega_N) + \alpha(\theta)\right]^{1/2}} d\theta \qquad (71)$$

The integration with respect to θ in equation (71) may be carried out in close form for a shallow spherical shell. For this case, the truncation error of center deflection PSD is:

$$\Delta\phi_W(\bar{\omega}_p, \omega_N) = 2\,\phi_o(\bar{\omega}_p)\,A^4\,\frac{ab}{\pi^2}\,\frac{1}{k_{1p}\,k_{2p}\left(\bar{\omega}_\rho^2 - \alpha\right)^2}$$

$$\left\{k_{1p}k_{2p}\,\frac{(a+b)}{\pi}\left[\frac{D}{\rho h}\left(\omega_N^2 - \alpha\right)\right]^{1/4}\left[\frac{1}{\left(\omega_N^2 - \alpha\right)^{1/2}} + \frac{\left(\omega_N^2 - \alpha\right)^{1/2}}{2\left(\omega_N^2 - \bar{\omega}_p^2\right)}\right.\right.$$

$$+ \frac{3}{4\left[\bar{\omega}_p^2 - \alpha\right]^{1/2}}\,\ell n\,\frac{\left(\bar{\omega}_p^2 - \alpha\right)^{1/2}\left(\omega_N^2 - \alpha\right)^{1/2} - \bar{\omega}_p^2 + \alpha}{\left(\bar{\omega}_p^2 - \alpha\right)^{1/2}\left(\omega_N^2 - \alpha\right)^{1/2} + \bar{\omega}_p^2 - \alpha}\Bigg] + \left[\frac{\omega_N\left(\bar{\omega}_p^2 - \alpha\right)}{\bar{\omega}_p\left(\omega_N^2 - \bar{\omega}_p^2\right)}\right.$$

$$\left.\left. - \frac{\alpha^{1/2}}{\bar{\omega}_p}\,\ell n\,\frac{\omega_N - \alpha^{1/2}}{\omega_N + \alpha^{1/2}} + \frac{\bar{\omega}_p^2 - \alpha}{2\bar{\omega}_p^2}\,\ell n\,\frac{\omega_N - \bar{\omega}_p}{\omega_N + \bar{\omega}_p}\right]\ell n\left[\frac{ab}{\pi^2}\left[\frac{\rho h}{D}\left(\omega_N^2 - \alpha\right)\right]^{1/2}\right]\right\} \qquad (72)$$

where $\alpha = E/(\rho R^2)$, $R = R_1 = R_2$, and the value of α is assumed to be smaller than the square of the lowest circular frequency. Based on equations (49) and (72), the relative error in response PSD due to truncation may be expressed in the following nondimensional form. In the formulation, equation (52) dealing with the natural frequencies has been made use of.

$$\epsilon(\bar{\omega}_o, \mu) = \gamma_p^2 p_1 p_2 \frac{1}{(1-\sigma)^2} \left\{ p_1 p_2 \frac{\pi(1+\bar{b})}{2\bar{b}} \left(\frac{\mu}{\bar{\omega}_o}\right)^{1/2} (1-\sigma\mu^2)^{-1/4} \left[1 + \frac{1-\mu^2\sigma}{2(1-\mu^2)} \right.\right.$$

$$+ \frac{3}{4\mu}\left(\frac{1-\mu^2\sigma}{1-\sigma}\right)^{1/2} \ell n \frac{(1-\sigma)^{1/2}(1-\mu^2\sigma)^{1/2} - \mu(1-\sigma)}{(1-\sigma)^{1/2}(1-\mu^2\sigma)^{1/2} + \mu(1-\sigma)} \left.\right] + \frac{1}{2}\left[\frac{\mu}{1-\mu^2}(1-\sigma) \right.$$

$$\left.\left. - \sigma^{1/2} \ell n \frac{1-\mu\sigma^{1/2}}{1+\mu\sigma^{1/2}} + \frac{1+\sigma}{2} \ell n \frac{1-\mu}{1+\mu} \right] \ell n \left[\frac{\bar{b}\bar{\omega}_o}{\pi^2\mu}(1-\mu^2\sigma)^{1/2} \right] \right\}$$

$$\left\{ 1 + 4\gamma_p^2 \sum_{\substack{\ell \\ \lambda_\ell \neq 1,\ \lambda_\ell \leq \mu^{-1}}} \frac{p_1 p_2 \left(2\lambda_\ell + p_1 p_2 / \ell_1 \ell_2\right)}{\ell_1 \ell_2 \left[\left(\lambda_\ell^2 - 1\right)^2 + 4\gamma_\ell^2 \lambda_\ell^2\right]} \right\}^{-1} \tag{73}$$

where

$\bar{\omega}_o = (\rho h/D)^{1/2} \bar{\omega}_p a^2$

$\bar{b} = b/a < 1$

$\sigma = \frac{\alpha}{\bar{\omega}_p^2} = \frac{12(1-\nu^2)}{\eta^2 \bar{h}^2 \bar{\omega}_o^2}$

$\eta = R/a >> 1$

$\mu = \bar{\omega}_p/\omega_N < 1$

$\lambda_\ell = \bar{\omega}_\ell/\bar{\omega}_p$

$\bar{h} = h/a$

Based on equation (73), the relative truncation errors of the fundamental mode for a spherical shallow element with $\gamma = 0.04$ are plotted in Figure 13 against μ^{-1} (the ratio of the cutoff frequency vs the natural frequency) corresponding to various curvature ratios a/R. The figure shows that the element with the smaller curvature ratio yields less errors. For a typical 48 inches by 36 inches by 0.118 inch steel panel with $\gamma = 0.04$, the relative errors of the fundamental modes are less than 0.1% when the cutoff frequency is only one and one-half times the natural frequency. Figure 14

shows the relative truncation errors of the (1, 1) and (3, 3) modes of a flat plate with different γ values (γ = 0.04, 0.01, 0.005). The figure indicates that the relative truncation errors are reduced with a reduced damping factor. It also shows that the error corresponding to a higher mode is larger than that of the lower mode when μ and γ are unchanged. Therefore, in order to retain a certain accuracy in the computed spectral data, the cutoff frequency should be chosen based on the relative error of the highest frequency of interest.

shows the relative truncation errors of the (1, 1) and (3, 3) modes of a flat plate with different γ values ($\gamma = 0.04, 0.01, 0.005$). The figure indicates that the relative truncation errors are reduced with a reduced damping factor. It also shows that the error corresponding to a higher mode is larger than that of the lower mode when μ and γ are unchanged. Therefore, in order to retain a certain accuracy in the computed spectral data, the cutoff frequency should be chosen based on the relative error of the highest frequency of interest.

D = bending rigidity of the plate or shell

g = loss factor

Z = impedance function of the plate or shell

The impedance functions Z are given below based on the simplified plate and shell equations:

1. Infinite plate (based on the classical plate equation):

$$Z = \left(k_1^2 + k_2^2\right)^2 - k_o^4 \tag{79}$$

where

$$k_o^4 = m\omega^2/D(1 + ig) \tag{80}$$

m = mass per unit area

2. Large shallow shell surface (a large shallow shell is one corresponding to which $a \gg h$, $a \gg \delta$, where a is the basic linear dimension of the shell, h is the thickness, and δ is the height of a typical arc on the shell middle surface):

$$Z = \left(k_1^2 + k_2^2\right)^2 - k_o^4 + 12(1 - \nu^2)/(Rh)^2 \tag{81}$$

where

R = radius of the spherical shell

h = thickness of the spherical shell

ν = Poisson's ratio

The deformation function $S_w(x, y, \omega)$ of the infinite plane, which is the inversed transformation of $F_w(k_1, k_2, \omega)$, may be obtained based on equations (75) and (77). The power spectral density of the deformation function w is given by

$$\phi_w(x, y, \omega) = \lim_{T \to \infty} \frac{1}{T} |S_w(x, y, \omega)|^2 \tag{82}$$

where 2T is the range of integration in the Fourier transform between ω, t.

An Infinite Plate Strip Under Random Acoustic Load

The problem involving an infinite plate strip or a semi-infinite plane may be solved through the introduction of line loads to the infinite plane. The line loads,

which may be transverse shear or bending moment, etc., are determined in such a manner that the displacement and stress distributions at the selected line location are identical to the boundary conditions of the plate strip or the semi-infinite plane. After the line loads are determined, the deformation function $F_w(k_1, k_2, \omega)$ in the wave number domain can be computed based on equation (77). In the following, a working example is presented which deals with the acoustic response of an infinite strip with two parallel simply supported edges.

The infinite strip, which is subjected to a uniform-intensity, spacewise correlated, and timewise random load, is shown in Figure 15(a). The loads acting on the corresponding infinite (x, y) plane which are used to simulate the plate strip are defined below:

1. Random acoustic loads

$$\begin{aligned} S_f(x, y, \omega) &= S_f(\omega) \qquad |x| \le \frac{1}{2} a, \ |y| \le \frac{1}{2} a \\ &= 0 \qquad\qquad |x| > \frac{1}{2} a \text{ or } |y| > \frac{1}{2} a \end{aligned} \tag{83}$$

2. Line force $P_1(y, \omega)$ and Line moment $M_1(y, \omega)$ along the lines $x = \pm \frac{1}{2} a (1 + \epsilon)$

where P_1 and M_1 are unknown functions which will be determined to satisfy the boundary conditions at $x = \pm \frac{1}{2} a$. We note that P_1, M_1 functions are delta functions along the x direction with unkown y distribution. The Fourier transform of the random load is

$$F_f(k_1, k_2, \omega) = \frac{1}{2\pi} \left\{ 2S_f(\omega) \frac{\sin \frac{1}{2} k_1 a \sin \frac{1}{2} k_2 a}{k_1 k_2} + \cos \frac{1}{2} k_1 a (1 + \epsilon) F_{P_1}(k_2, \omega) \right.$$

$$\left. + k_1 \sin \frac{1}{2} k_1 a (1 + \epsilon) F_{M_1}(k_2, \omega) \right\} \tag{84}$$

Since the geometry and the applied loads on the plate are symmetric w.r.t. the y-axis, the simply supported boundary conditions may be reduced to two which involve two unknown functions $F_{P_1}(k_2, \omega)$ and $F_{M_1}(k_2, \omega)$ as follows:

$$2S_f(\omega) \frac{\sin \frac{1}{2} k_2 a}{k_2} I_1(k_2) + F_{P_1}(k_1, \omega) I_2(k_2) + F_{M_1}(k_1, \omega) I_3(k_1) = 0 \tag{85}$$

$$2S_f(\omega)\,\frac{\sin\frac{1}{2}k_2a}{k_2}\,I_3(k_2) + F_{P_1}(k_2,\omega)\,I_4(k_2) + F_{M_1}(k_2,\omega)\,I_5(k_2) = 0 \qquad (86)$$

where

$$I_1(k_2) = \frac{\pi}{4k_o^2}\,\frac{1}{\eta_1^2\eta_2^2}\left[\eta_2^2(1-e^{-\eta_1 a}) - \eta_1^2(1+e^{-\eta_2 a})\right] \qquad (87)$$

$$I_2(k_2) = \frac{\pi}{4k_o^2}\,\frac{1}{\eta_1\eta_2}\left[\eta_2(1+e^{-\eta_1 a}) - \eta_1(1+e^{-\eta_2 a})\right] \qquad (88)$$

$$I_3(k_2) = \frac{\pi}{4k_o^2}\left|e^{-\eta_1 a} - e^{-\eta_2 a}\right| \qquad (89)$$

$$\left[I_4(k_2) = \frac{\pi}{4k_o^2}\left[\eta_2(1+e^{-\eta_2 a}) - \eta_1(1+e^{-\eta_1 a})\right]\right. \qquad (90)$$

$$\left[I_5(k_2) = \frac{\pi}{4k_o^2}\left[\eta_1^2(1+e^{-\eta_1 a}) + \eta_2^2(1+e^{-\eta_2 a})\right]\right. \qquad (91)$$

and

$$\eta_1 = \sqrt{k_2^2 - k_o^2}$$

$$\eta_2 = \sqrt{k_2^2 + k_o^2}$$

$$k_o^4 = \frac{m\omega^2}{D(1+ig)} \simeq \frac{m\omega^2}{D}(1-ig) \qquad g \ll 1$$

The above equations lead to:

$$F_{P_1}(k_2,\omega) = 2S_f(\omega)\,\frac{\sin\frac{1}{2}k_2a}{k_2}\,\frac{1}{\eta_2-\eta_1}\left[\frac{\eta_1}{\eta_2}\tanh\eta_2 - \frac{\eta_2}{\eta_1}\tanh\eta_1\right] \qquad (92)$$

$$F_{M_1}(k_2,\omega) = 2S_f(\omega)\,\frac{\sin\frac{1}{2}k_2a}{k_2}\,\frac{\eta_1}{\eta_2-\eta_1}\left[\frac{1}{\eta_1}\tanh\eta_1 - \frac{1}{\eta_2}\tanh\eta_2\right] \qquad (93)$$

Based on equation (77), (84), (92), and (93), the Fourier transform of the deformation function $F_w(k_1, k_2, \omega)$ of the infinite strip is obtained.

Plates and Shallow Shells of Finite Dimensions Under Random Acoustic Loads

The finite plate or shallow shell may be treated in a similar manner as that of the infinite plate strip. In dealing with the finite plate, the line load functions at the boundaries are to be determined iteratively. This is because of the coupling between the line functions at intersecting boundaries.

We have performed analysis along the scheme described above. It seems that there are certain shortcomings inherent in the approach dealing with a finite structure where the Fourier transformation from the space domain to the wave number domain is carried out. The shortcomings include:

1. The need of iteration in determining the line functions at the boundary
2. Poor convergence
3. Lengthy numerical computations
4. Complicated integral evaluation.

In the following, a working example is presented which deals with the random vibration of a square plate with simply supported edges. The plate is under a uniform intensity, spacewise correlated, and timewise random load (Figure 15(b)).

The Fourier transform of the load is:

$$F_f(k_1, k_2, \omega) = \frac{1}{2\pi}\left\{2S_f(\omega)\,\frac{\sin\frac{1}{2}k_1 a \sin\frac{1}{2}k_2 a}{k_1 k_2} + \cos\frac{1}{2}k_1 a(1+\epsilon)\,F_P(k_2, \omega)\right.$$

$$+ k_1 \sin\frac{1}{2}k_1 a(1+\epsilon)\,F_M(k_2,\omega) + \cos\frac{1}{2}k_2 a(1+\epsilon)\,F_P(k_1,\omega)$$

$$\left. + k_2 \sin\frac{1}{2}k_2 a(1+\epsilon)\,F_M(k_1,\omega)\right\} = F_f(k_2, k_1, \omega) \qquad (94)$$

Since the geometry and the applied loads on the plate are doubly symmetric to the x and y axes, the simply supported boundary conditions may be reduced which involve two unknown functions $F_P(k_2, \omega)$ and $F_M(k_2, \omega)$ as follows:

$$2\,S_f(\omega)\,\frac{\sin\frac{1}{2}k_2a}{k_2}\,I_3(k_2)+F_P(k_2,\omega)\,I_4(k_2)+F_M(k_2,\omega)\,I_5(k_2)$$
$$+\cos\tfrac{1}{2}k_2a\,(I+\epsilon)\int_{-\infty}^{\infty}\frac{k_1^{\,2}F_P(k_1,\omega)}{Z}\,e^{\,i\frac{1}{2}k_1a}\,dk_1$$
$$+k_2\sin\tfrac{1}{2}k_2a\,(I+\epsilon)\int_{-\infty}^{\infty}\frac{k_1^{\,2}F_M(k_1,\omega)}{Z}\,e^{\,i\frac{1}{2}k_1a}\,dk_1=0 \qquad (95)$$

$$2\,S_f(\omega)\,\frac{\sin\frac{1}{2}k_2a}{k_2}\,I_1(k_2)+F_P(k_2,\omega)\,I_2(k_2)+F_M(k_2,\omega)\,I_3(k_2)$$
$$+\cos\tfrac{1}{2}k_2a\,(I+\epsilon)\int_{-\infty}^{\infty}\frac{F_P(k_1,\omega)}{Z}\,e^{\,i\frac{1}{2}k_1a}\,dk_1$$
$$+k_2\sin\tfrac{1}{2}k_2a\,(I+\epsilon)\int_{-\infty}^{\infty}\frac{F_M(k_1\,\omega)}{Z}\,e^{\,i\frac{1}{2}k_1a}\,dk_1=0 \qquad (96)$$

For a first approximation, it may be assumed that the influence of a line load on the boundary conditions is most significant to the boundary at which the line load is located or otherwise is parallel to the line load. The effect is less significant to a boundary which is perpendicular to the line load. By ignoring the above described secondary effect in a first approximation, the problem is reduced to that of an infinitely long plate strip with width a and simply supported edges along $x = \pm\frac{1}{2}a$. It is subjected to the half-surface loads $S_f(\omega)$. In this manner, $F_P(k_2, \omega)$ and $F_M(k_2, \omega)$ are equal to one-half of the value F_{P_1} and F_{M_1} as given in equations (92) and (93).

The second iternation may be initiated as follows:

$$\begin{cases} F_P(k_2,\omega) = F_{P_1}(k_2,\omega) + F_\alpha(k_2,\omega) & (97) \\ F_M(k_2,\omega) = F_{M_1}(k_2,\omega) + F_\beta(k_2,\omega) & (98) \end{cases}$$

where $\frac{1}{2}F_{P_1} + F_\alpha$ and $\frac{1}{2}F_{M_1} + F_\beta$ are the corrections on the first approximated solution $\frac{1}{2}F_{P_1}(k_2, \omega)$ and $\frac{1}{2}F_{M_1}(k_2, \omega)$. Substituting equations (97), (98) into equations (95), (96) and dropping the integrals which involve F_α and F_β gives the two equations

governing the corrections F_α (k_2, ω) and F_β (k_2, ω). These equations are very lengthy and are detailed as equations (99), (100) on the next page. The integrals in equations (99), (100) are evaluated by the residue theorem before the two simultaneous equations are solved. The numerical result shows that the corrected terms F_α and F_β are of the same order of magnitude of F_{P_1} and F_{M_1}. Because of the complicated integral evaluation, the lengthy numerical computation, and the poor convergence property of the problem, no additional iteration was carried out beyond the second round.

$$
\begin{cases}
I_2(k_2)\,F_\alpha(k_2) + I_3(k_2)\,F_\beta(k_2) \\
\quad + 2k_o^2 \cos\frac{k_2 a}{2} \int_{-\infty}^{\infty} \dfrac{\sin\frac{k_1 a}{2}\,\sinh\frac{q_1 a}{2}\,\sinh\frac{q_2 a}{2}}{k_1 q_1 q_2\left[q_1 \sinh\frac{q_1 a}{2}\cosh\frac{q_2 a}{2} - q_2\cosh\frac{q_1 a}{2}\sinh\frac{q_2 a}{2}\right]\left[\left(k_1^2 + k_2^2\right) - k_o^4\right]} e^{i\frac{1}{2}k_1 a}\,dk_1 \\
\quad + k_2 \sin\frac{k_2 a}{2} \int_{-\infty}^{\infty} \dfrac{\sin\frac{k_1 a}{2}\left[q_2 \sinh\frac{q_1 a}{2}\cosh\frac{q_2 a}{2} - q_1\cosh\frac{q_1 a}{2}\sinh\frac{q_2 a}{2}\right]}{k_1 q_1 q_2\left[q_1 \sinh\frac{q_1 a}{2}\cosh\frac{q_2 a}{2} - q_2\cosh\frac{q_1 a}{2}\sinh\frac{q_2 a}{2}\right]\left[\left(k_1^2 + k_2^2\right) - k_o^4\right]} e^{i\frac{1}{2}k_1 a}\,dk_1 = 0 \qquad (99) \\
I_4(k_2)\,F_\alpha(k_2) + I_5(k_2)\,F_\beta(k_2)
\end{cases}
$$

$$
\begin{aligned}
&+ 2k_o^2 \cos\frac{k_2 a}{2} \int_{-\infty}^{\infty} \frac{k_1 \sin\frac{k_1 a}{2}\,\sinh\frac{q_1 a}{2}\,\sinh\frac{q_2 a}{2}}{q_1 q_2\left[q_1 \sinh\frac{q_1 a}{2}\cosh\frac{q_2 a}{2} - q_2\cosh\frac{q_1^2}{2}\sinh\frac{q_2 a}{2}\right]\left[\left(k_1^2 + k_2^2\right) - k_o^4\right]} e^{i\frac{1}{2}k_1 a}\,dk_1 \\
&+ k_2 \sin\frac{k_2 a}{2} \int_{-\infty}^{\infty} \frac{k_1 \sin\frac{k_1 a}{2}\left[q_a \sinh\frac{q_1 a}{2}\cosh\frac{q_2 a}{2} - q_1\cosh\frac{q_1 a}{2}\sinh\frac{q_2 a}{2}\right]}{q_1 q_2\left[q_1 \sinh\frac{q_1 a}{2}\cosh\frac{q_2 a}{2} - q_2\cosh\frac{q_1 a}{2}\sinh\frac{q_2 a}{2}\right]\left[\left(k_1^2 + k_2^2\right) - k_o^4\right]} e^{i\frac{1}{2}k_1 a}\,dk_1 = 0 \qquad (100)
\end{aligned}
$$

where $q_1 = \sqrt{k_1^2 - k_o^2}$

$q_2 = \sqrt{k_1^2 + k_o^2}$

REFERENCES

1. Lyon, R.H., and Maidanik, G., "Power Flow Between Linearly Coupled Oscillators," J. Acoust. Soc. Am. 34, 623-639, May 1962.

2. Smith, P.W., Jr., "Response and Radiation of Structural Modes Excited by Sound," J. Acoust. Soc. Am. 34, 827, 1962.

3. Maidanik, G., "Response of Ribbed Panels to Reverberant Acoustic Fields," J. Acoust. Soc. Am. 34, 809-826, 1962.

4. Lyon, R.H., and Eichler, E., "Random Vibration of Connected Structures," J. Acoust. Soc. Am. 36, 1344-1354, July 1964.

5. Crocker, M.J., and Price, A.J., "Sound Transmission Using Statistical Energy Analysis," J. Sound and Vibration, 9 (3), 469-486, September 1969.

6. Lyon, R.H., "An Energy Method for Prediction of Noise and Vibration Transmission," Shock, Vibr. and Assoc. Environments, Bull. No. 33, Pt. II, pp. 13-25, 1964.

7. Lyon, R.H., and Maidanik, G., "Statistical Methods in Vibration Analysis," AIAA Journal 2, 1015-1024, June 1964.

8. Smith, P.W., Jr., and Lyon, R.H., "Sound and Structural Vibration," NASA CR-160, March 1965.

9. Lyon, R.H., and Scharton, T.D., "Vibrational-Energy Transmission in a Three-Element Structure," J. Acoust. Soc. Am. 38, 253-261, August 1965.

10. Eichler, E., "Thermal Circuit Approach to Vibrations in Coupled Systems and the Noise Reduction of a Rectangular Box," J. Acoust. Soc. Am. 37, 995-1007, 1965.

11. Ungar, E.E., "Fundamentals of Statistical Energy Analysis of Vibrating Systems," AFFDL-TR-66-52, May 1966.

12. Ungar, E.E., "Mechanical Vibrations," Sec. 6 of Mechanical Design and Systems Handbook, McGraw-Hill Book Co., Inc., New York, 1964.

13. Ungar, E.E., "Statistical Energy Analysis of Vibrating Systems," J. Eng. Ind. 89, No. 4, 626-632, 1967.

14. Lyon, R.H., "Statistical Analysis of Power Injection and Response in Structures and Rooms," J. Acoust. Soc. Am. 45, 545-563, March 1969.

15. Noiseux, D.U., "Measurement of Power Flow in Uniform Beams and Plates, J. Acoust. Soc. Am. 47, 238-247, January 1970.

16. Zeman, J.L., and Bogdanoff, J.L., "A Comment on Complex Structural Response to Random Vibrations," AIAA Journal 7, 7, 1225-1231, July 1969.

17. Newland, D.E., "Calculation of Power Flow Between Coupled Oscillators," J. Sound Vib. 3, 262-276, 1966.

18. Newland, D.E., "Power Flow Between a Class of Coupled Oscillators," J. Acoust. Soc. Am. 43, 553-565, March 1968.

19. Heckl, M.A., "Wave Propagation on Beam-Plate Systems," J. Acoust. Soc. Am. 33, 640-651, 1961.

20. Ungar, E.E., "Transmission of Plate Flexural Waves through Reinforcing Beams; Dynamic Stress Concentrations," J. Acoust. Soc. Am. 33, 633-639, 1961.

21. Manning, J.E., and Maidanik, G., "Radiation Properties of Cylindrical Shells," J. Acoust. Soc. Am. 36, 1691-1698, 1964.

22. Lyon, R.H., "Spatial Response Concentrations in Extended Structures," Trans. ASME, J. Eng. for Ind., Series B, 1967.

23. Dyer, I., "Response of Space Vehicle Structures to Rocket Engine Noise," Ch. 7 of Random Vibration, Vol. 2, Ed. by S.H. Crandall, The MIT Press, Cambridge, Massachusetts, 1963.

24. Skudrzyk, E., "Vibrations of a System with a Finite or an Infinite Number of Resonances," J. Acoust. Soc. Am. 30, 1140-1152, 1958.

25. Kronauer, R.E., and Musa, S.A., "Exchange of Energy Between Oscillations in Weakly Nonlinear Conservative Systems, J. Appl. Mech. 33, No. 2, 451-452, 1966.

26. Franken, P.A., and Lyon, R.H., "Estimation of Sound-Induced Vibrations by Energy Methods, with Applications to the Titan Missile," Shock, Vibration, and Associated Environments, Bull. No. 31, Part III, pp. 12-26, 1963.

27. Heckl, M.A., "Measurements of Absorption Coefficients on Plates," J. Acoust. Soc. Am. 34, 803-808, 1962.

28. Lyon, R.H., "What Good Is Statistical Energy Analysis, Anyway?" Shock and Vibration Digest, Vol. 2, No. 6, June 1970.

29. Kana, D.D., Chu, W.H., and Bessey, R.L., "The Response of Cylindrical Shells to Random Acoustic Excitation Over Broad Frequency Ranges," AIAA Paper 71-331, April 1971.

30. Cobble, M.H., "Finite Transform Solution of the Damped Clamped-Clamped Beam Having Distributed Load and Elastic Support, J. Acoust. Soc. Am. 40, 1529-1533, December 1966.

31. Hurty, W.C., and Rubinstein, M.F., Dynamics of Structures, Prentice-Hall, Inc., Englewood Cliffs, New Jersey, First Edition, 1965.

32. Nowacki, W., Dynamics of Elastic Systems, John Wiley and Sons, New York, First Edition, 1963.

33. Hwang, C., and Pi, W.S., "Random Acoustic Response of a Cylindrical Shell," AIAA Journal 7, 12, 2204-2210, December 1969.

34. Courant, R., and Hilbert, D., Methods of Mathematical Physics, Interscience Publishers, Inc., New York, N.Y., 1953, Vol. I, Chapter 6, pp. 429-431, 460.

35. Bolotin, V.V., "On the Density of the Distribution of Natural Frequencies of Thin Elastic Shells," J. Appl. Math. and Mech. 27, No. 2, 538-543 (Transl. from Soviet Journal: Prikhadnaya Matematika y Mekhanika, 27, No. 2, pp. 362-364), 1963.

36. Bolotin, V.V., "The Density of Eigenvalues in Vibration Problems of Elastic Plates and Shells," Proc. of Vibration Problems, Warsaw 4, No. 6, 341-351, 1965.

37. Wilkinson, J.P.D., "Modal Densities of Certain Shallow Structural Elements," J. Acoust. Soc. Am., Vol. 43, No. 2, pp. 245-251, February 1968.

38. Sneddon, I.N., Fourier Transforms, McGraw-Hill Company, New York, 1951.

39. Bendat, J.S., and Piersol, J.S., Measurement and Analysis of Random Data, J. Wiley and Sons, Inc., New York, 1966.

40. Powell, A., "On the Response of Structures to Random Pressures and to Jet Noise in Particular," Ch. 8 of Random Vibration, Vol. I, Ed. by S.H. Crandall, The MIT Press, Cambridge, Massachusetts, 1963.

41. Bolotin, V.V., "The Edge Effect in the Oscillations of Elastic Shells," PMM 24, No. 5, pp. 831-834 (translation pp. 1257-1272), 1960.

42. Bolotin, V.V., Makarov, B.P., Mishenkov, G.V., and Shveiko, Iu. Iu., "An Asymptotic Method for the Study of Natural Frequencies of Elastic Plates," Sbornik Raschety na Prochnost', Vol. 6, Mashgiz, 1960 (in Russian).

43. Hart, F. D., and Desai, V. D., "Additive Property of Modal Density for a Composite Structure," J. Acoust. Soc. Am. 42, 1203, November 1967.

44. Jacobs, L. D., and Lagerquist, D. R., "Finite Element Analysis of Complex Panel Response to Random Loads," AFFDL-TR-68-44, October 1968.

45. Morse, P. M., and Ingard, K. U., Theoretical Acoustics, McGraw-Hill Book Co., New York, 1968.

LIST OF ILLUSTRATIONS

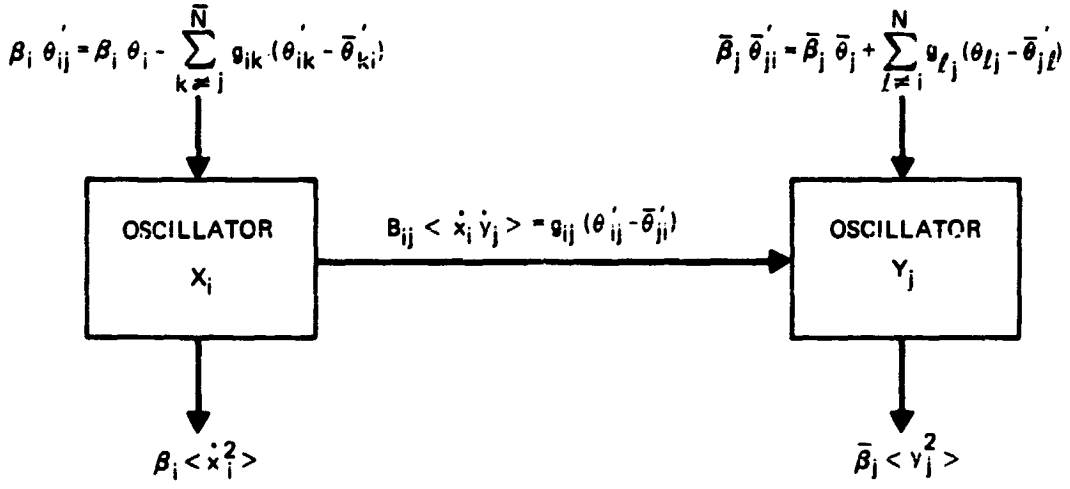

FIGURE 1. ENERGY FLOW IN COUPLED OSCILLATORS OF TWO SUBSTRUCTURES

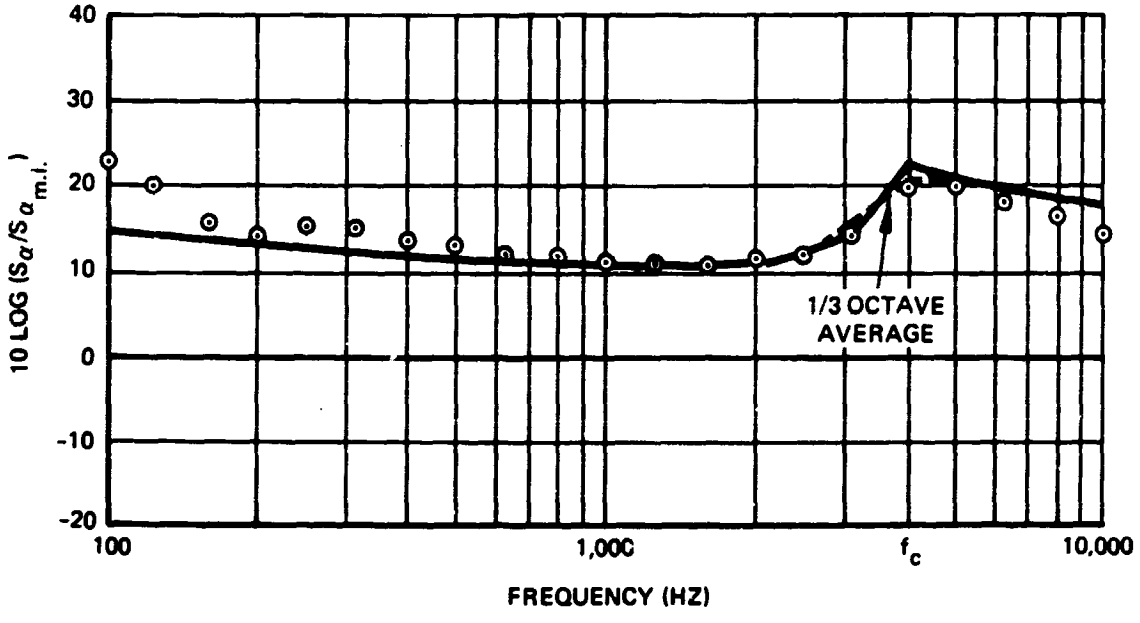

FIGURE 2. PANEL RESPONSE RELATIVE TO MASS LAW. $\eta_{int} = 0.005$ (FROM REFERENCE 5)

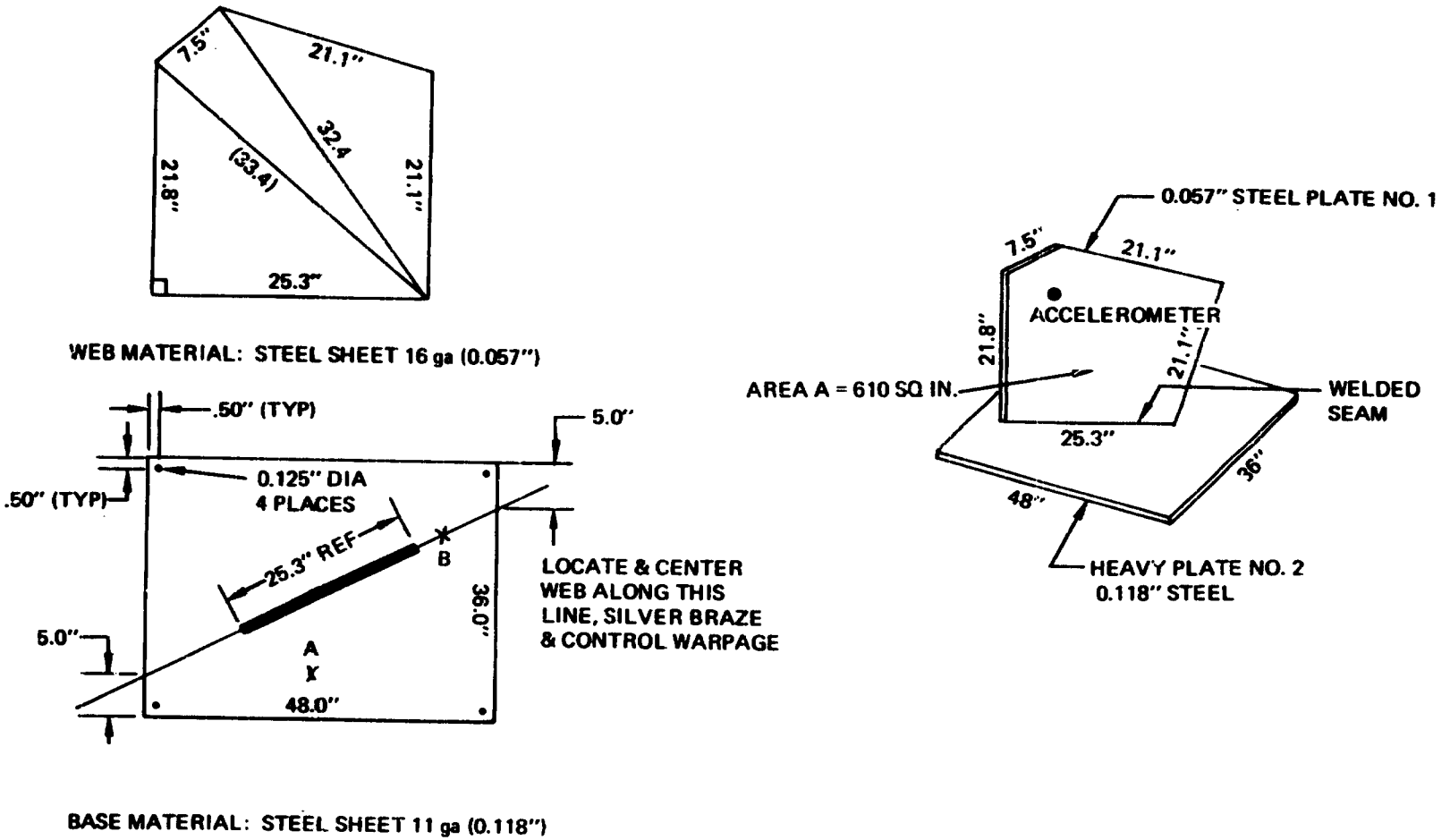

FIGURE 3. TWO PLATE TEST SPECIMEN (AFTER REFERENCE 4)

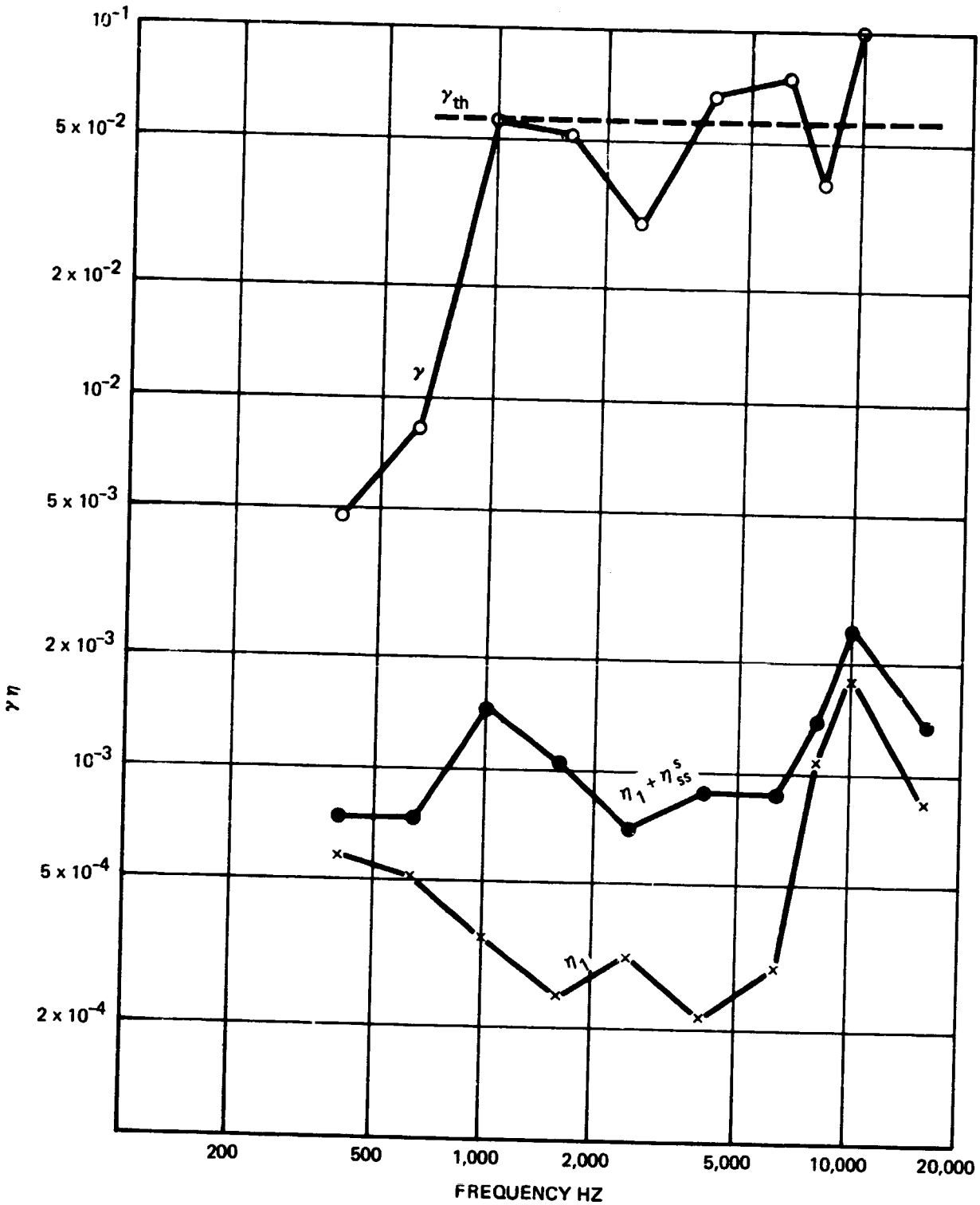

FIGURE 4. LOSS FACTORS AND ABSORPTION COEFFICIENT OF UNDAMPED 57-MIL STEEL PLATE WELDED TO 118-MIL PLATE (FROM REFERENCE 4)

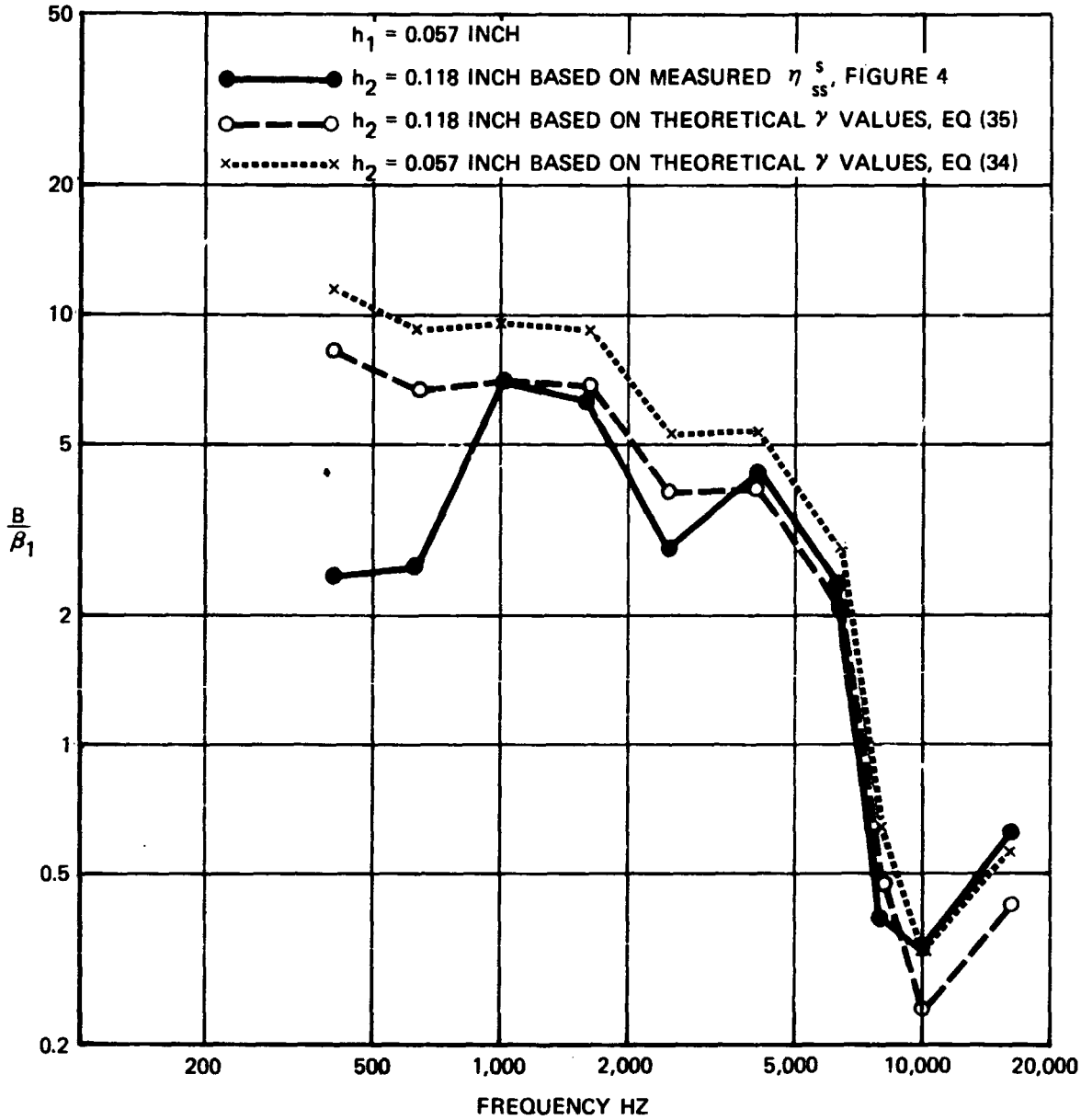

FIGURE 5. RATIO OF (DAMPING COUPLING PARAMETER/MODAL DAMPING COEFFICIENT) FOR THE TWO-PLATE SYSTEM

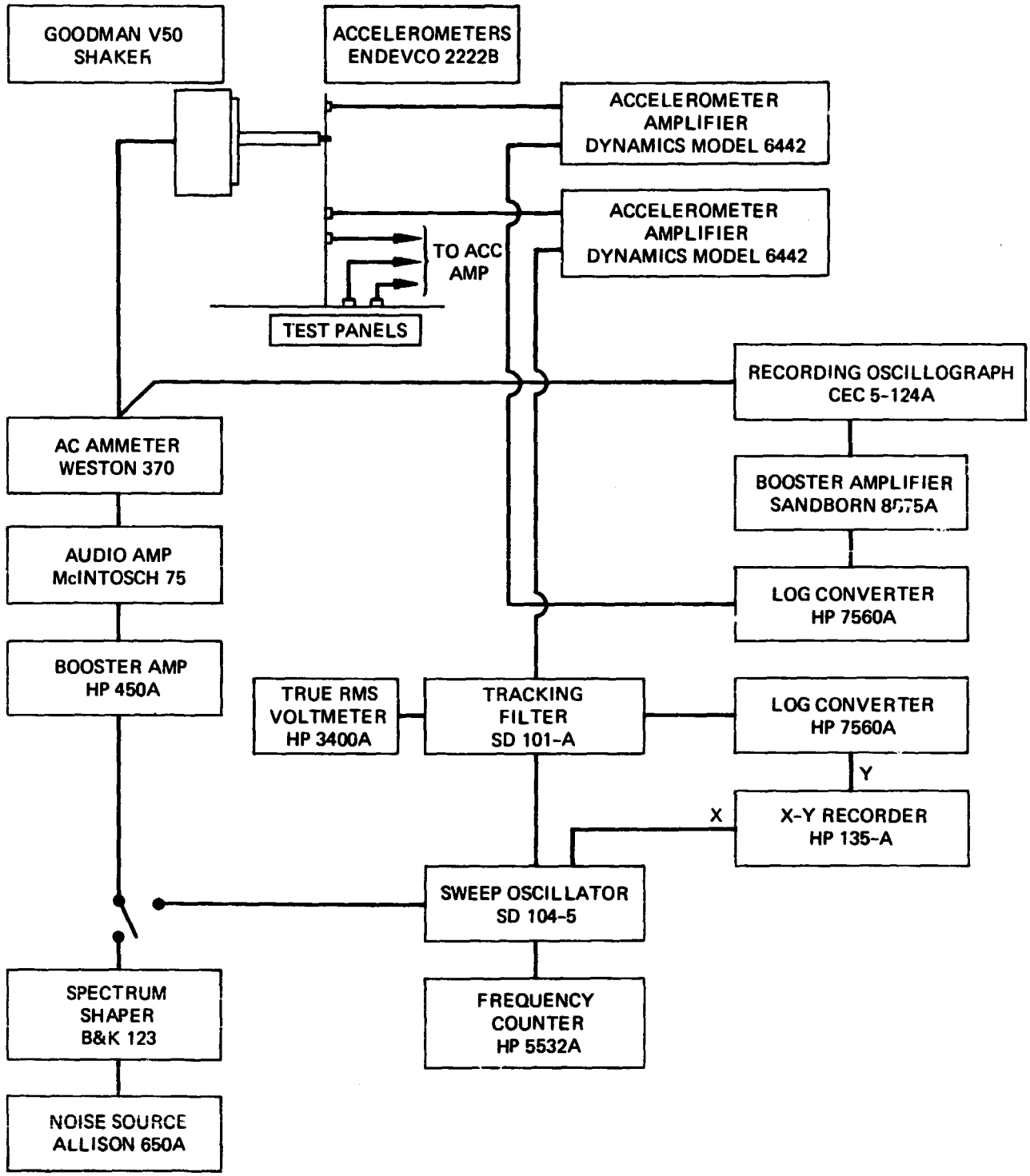

FIGURE 6. INSTRUMENTATION SYSTEM SCHEMATIC

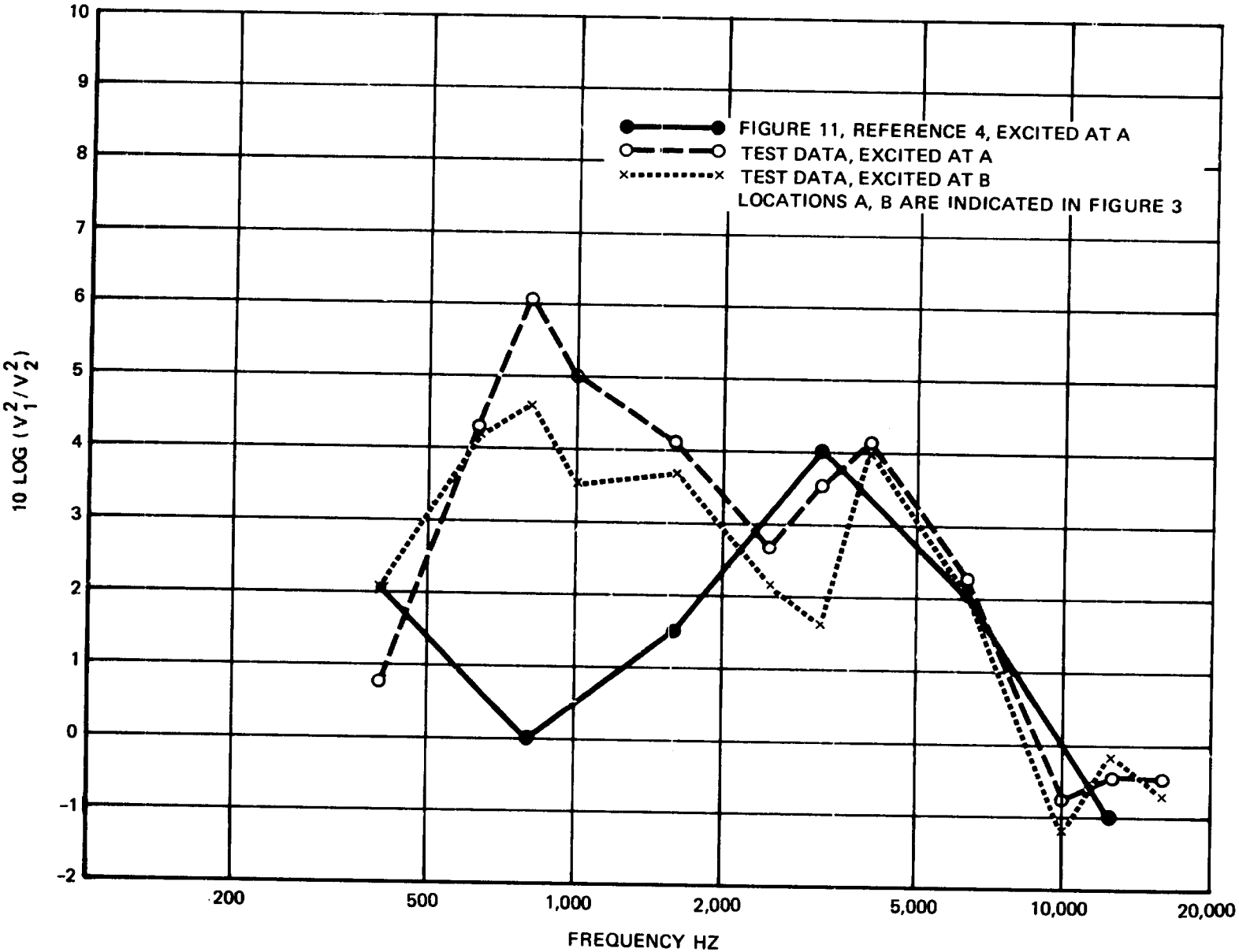

FIGURE 7. RESPONSE RATIOS FOR UNDAMPED 57-MIL PLATE WELDED TO 118-MIL PLATE

7101362A

FIGURE 8. DEFORMATION PATTERN OF THE BASE PLATE UNDER SINUSOIDAL EXCITATION, f = 4000 Hz

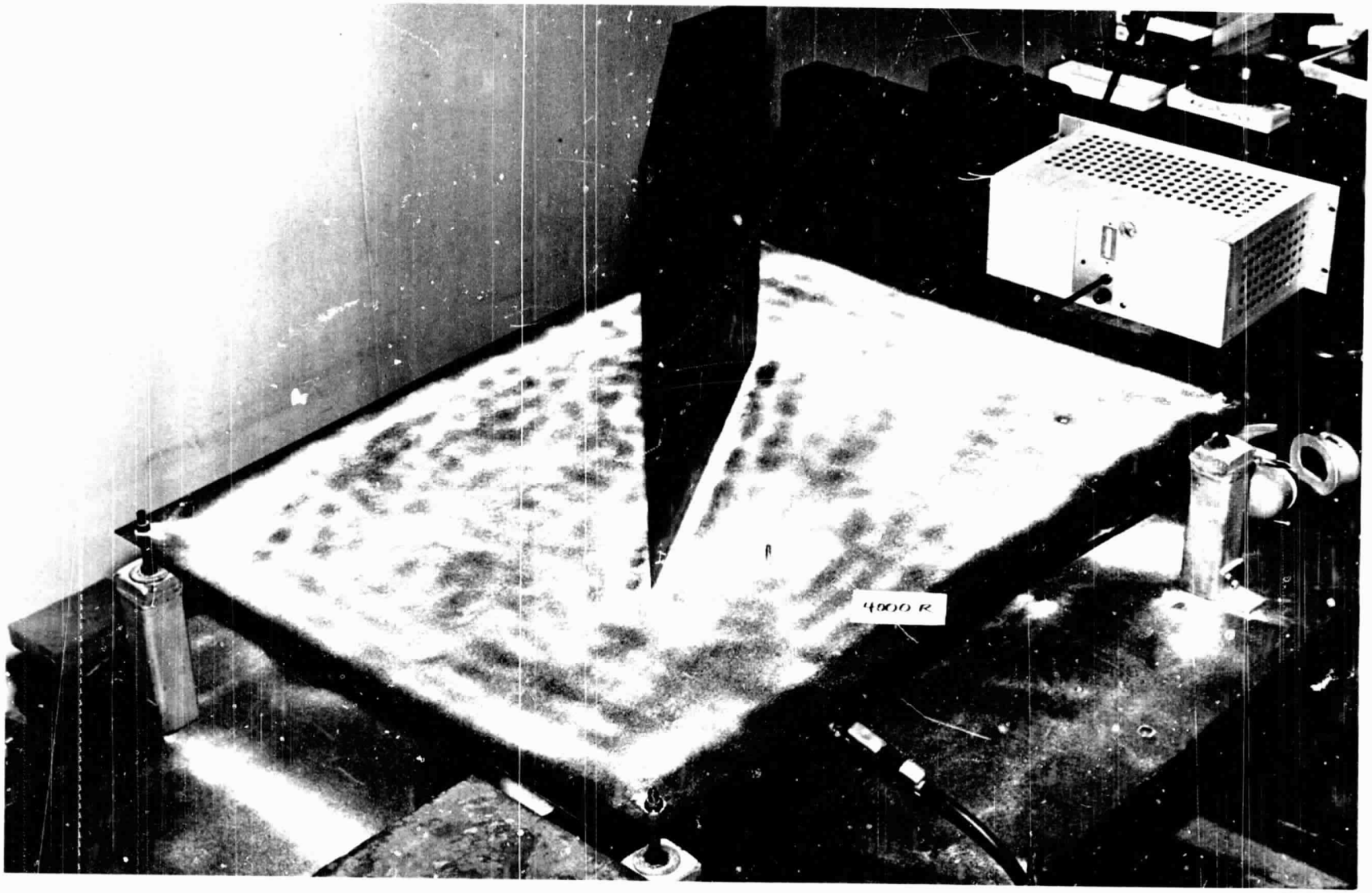

7101362B

FIGURE 9. DEFORMATION PATTERN OF THE BASE PLATE UNDER 1/3 OCTAVE EXCITATION, f_o = 4000 Hz

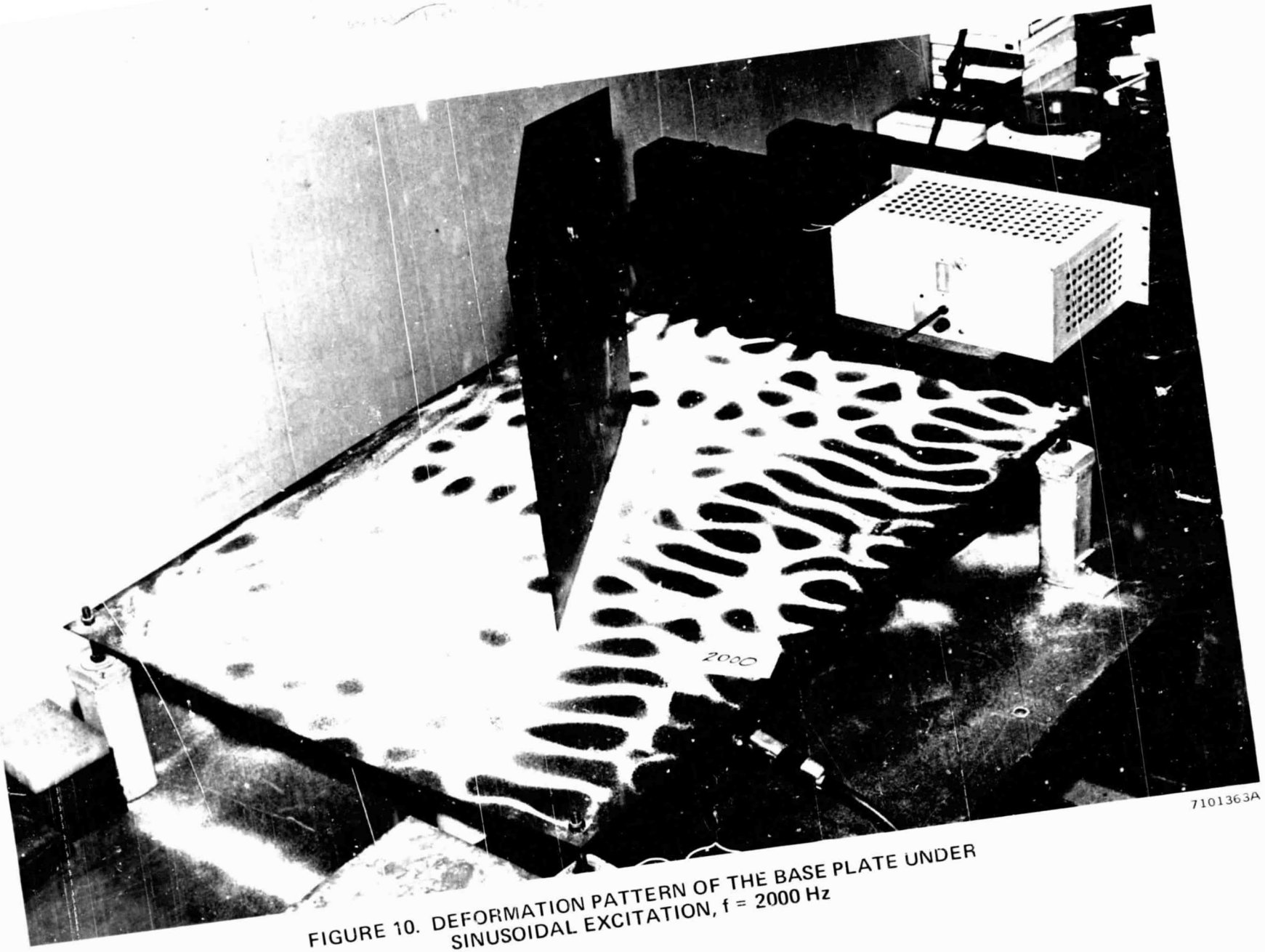

FIGURE 10. DEFORMATION PATTERN OF THE BASE PLATE UNDER SINUSOIDAL EXCITATION, f = 2000 Hz

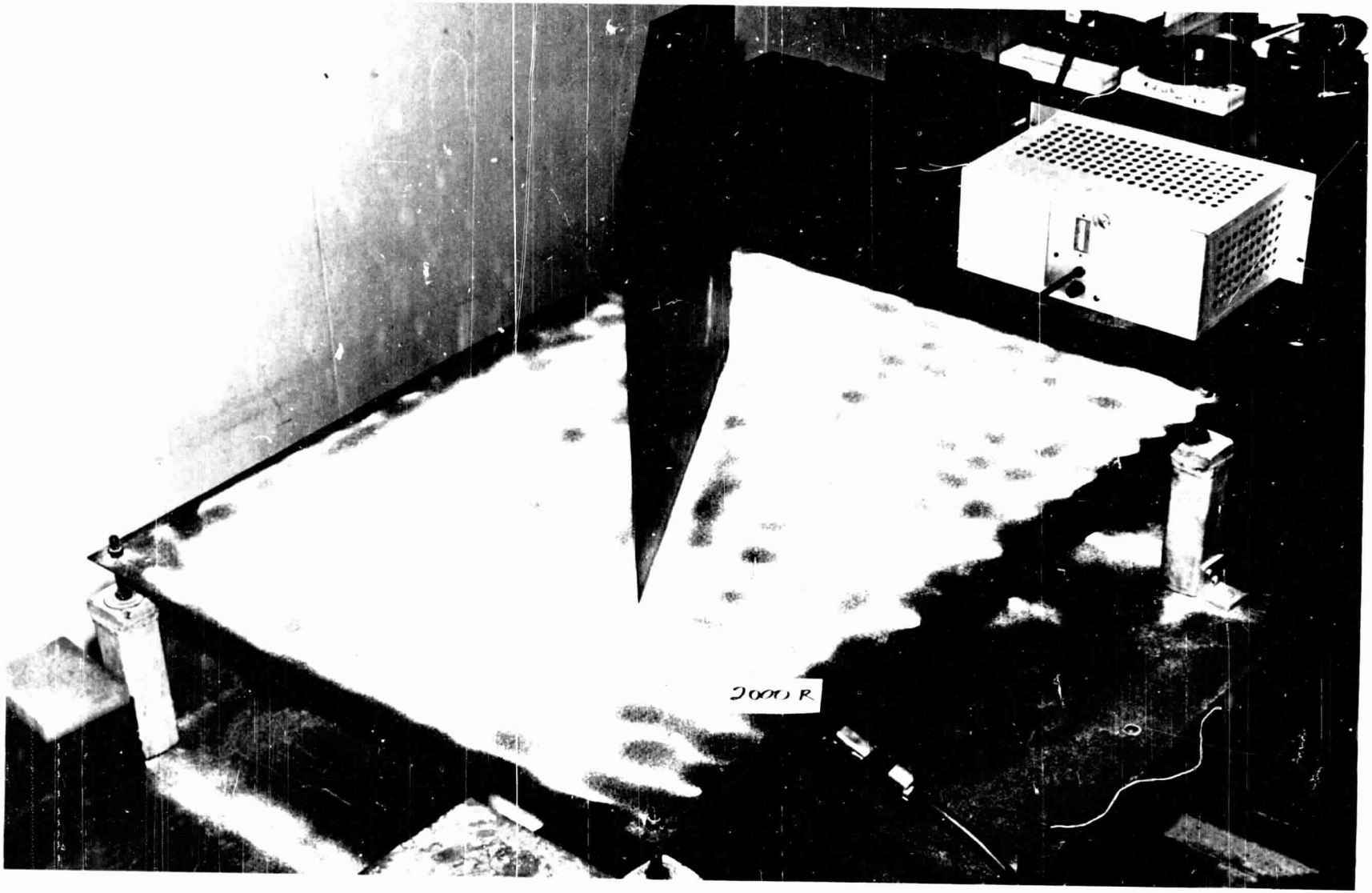

7101363B

FIGURE 11. DEFORMATION PATTERN OF THE BASE PLATE UNDER 1/3 OCTAVE EXCITATION, f_o = 2000 Hz

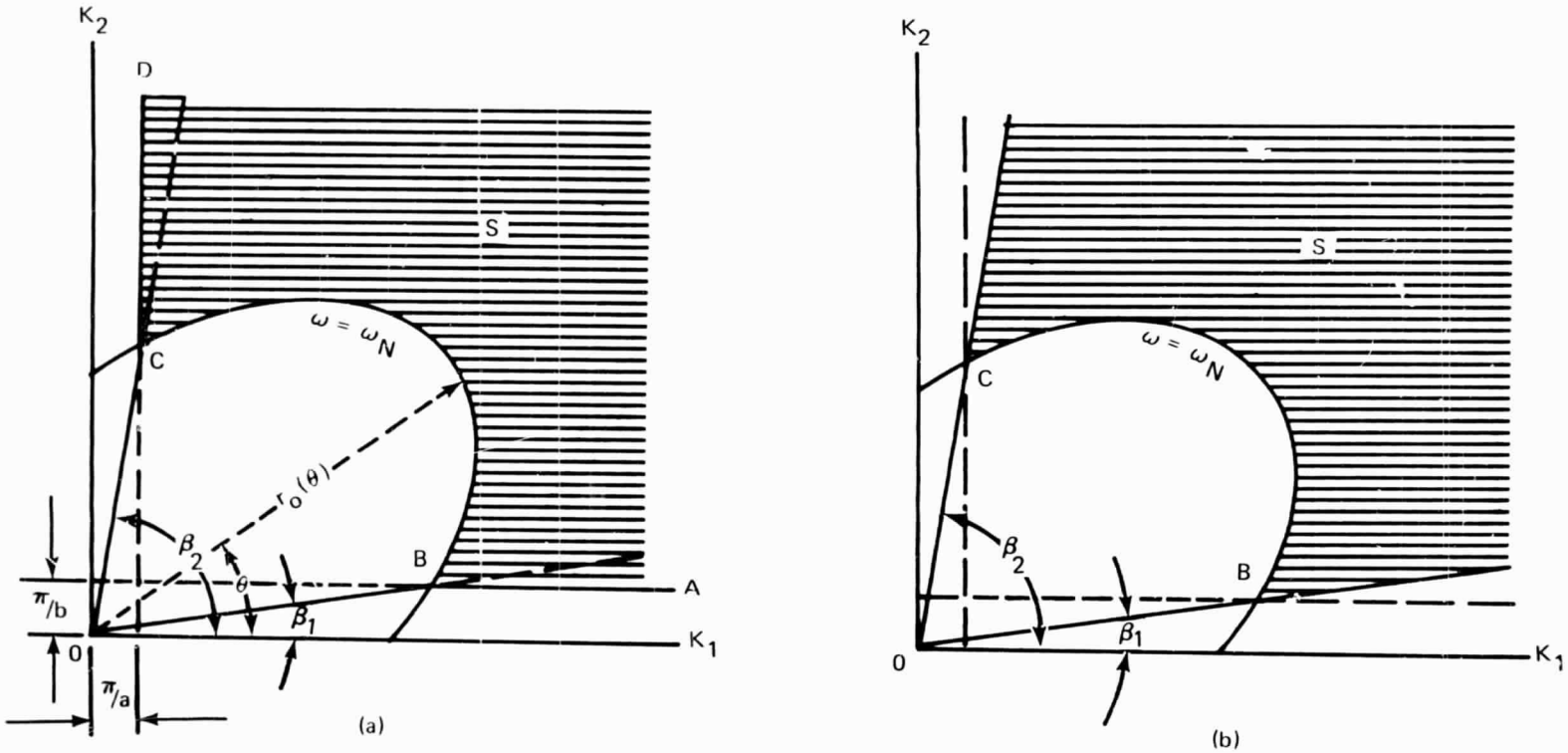

FIGURE 12. MODAL DISTRIBUTION OF A DOUBLE CURVED SHALLOW SHELL ELEMENT IN THE WAVE NUMBER DOMAIN

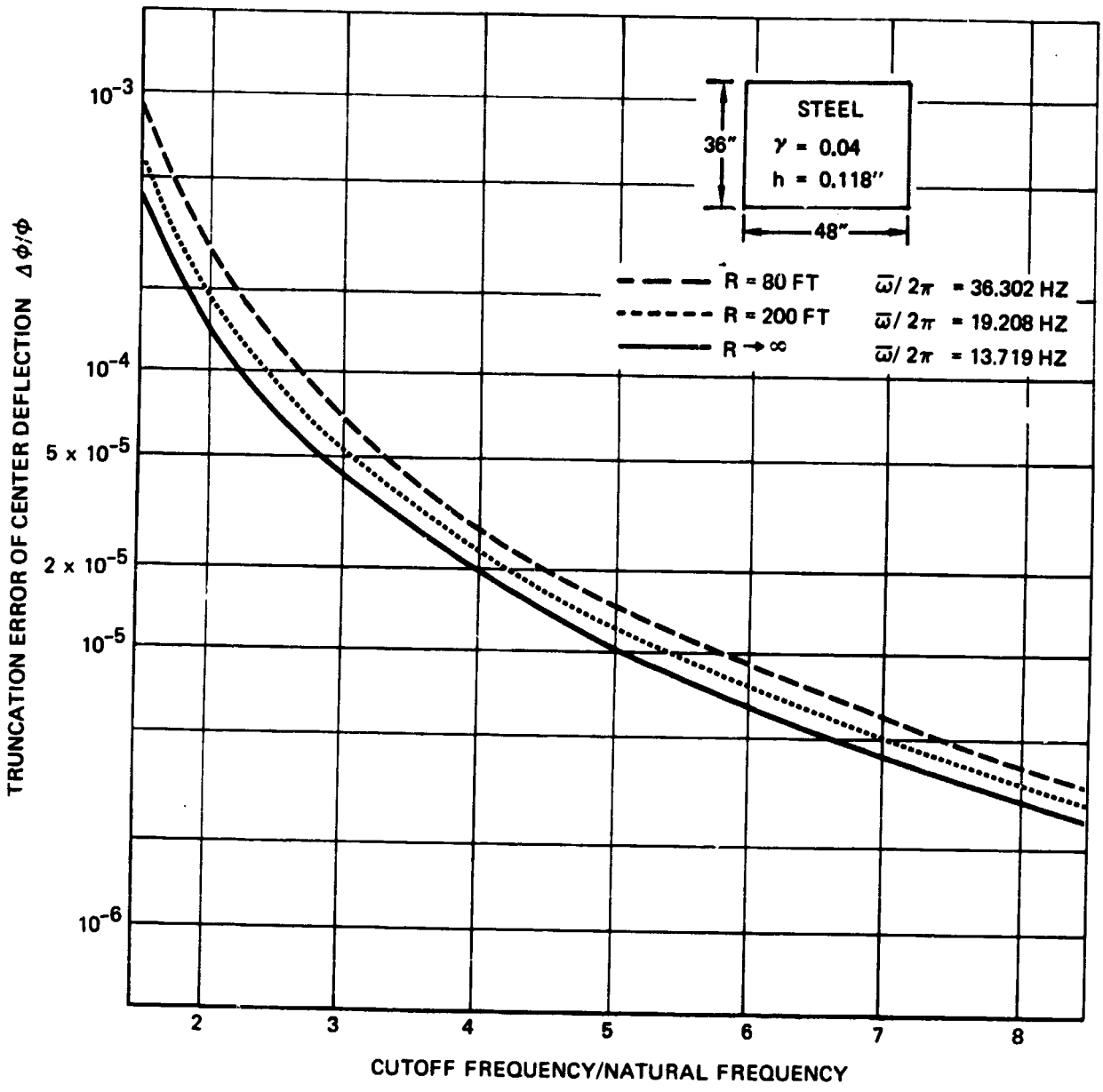

FIGURE 13. TRUNCATION ERRORS OF THE CENTER DEFLECTIONS OF SIMPLY SUPPORTED SHALLOW SPHERICAL PANELS UNDER UNIFORM INTENSITY ACOUSTIC PRESSURE

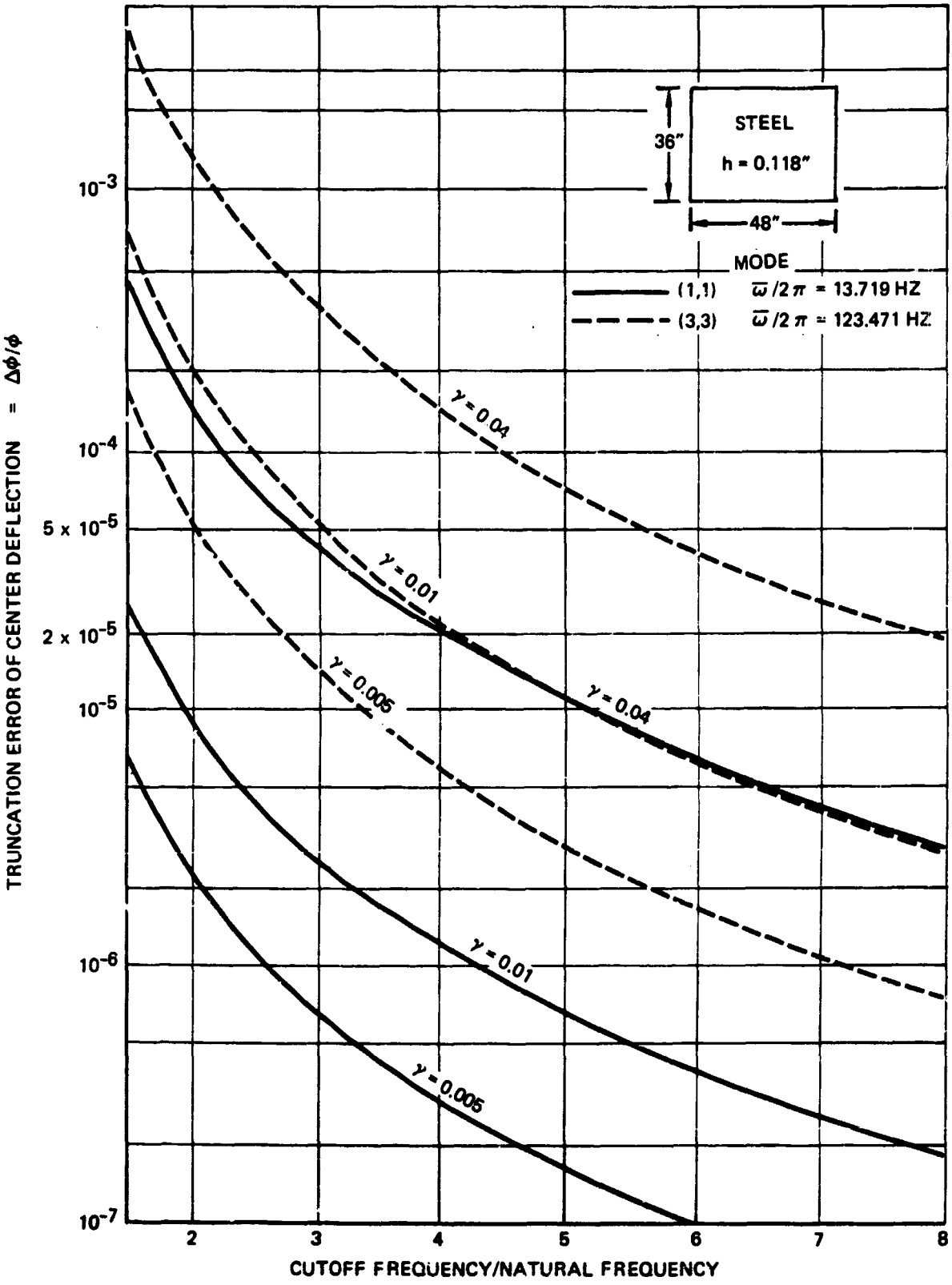

FIGURE 14. TRUNCATION ERRORS OF CENTER DEFLECTION OF A SIMPLY SUPPORTED PLATE UNDER UNIFORM INTENSITY ACOUSTIC PRESSURE

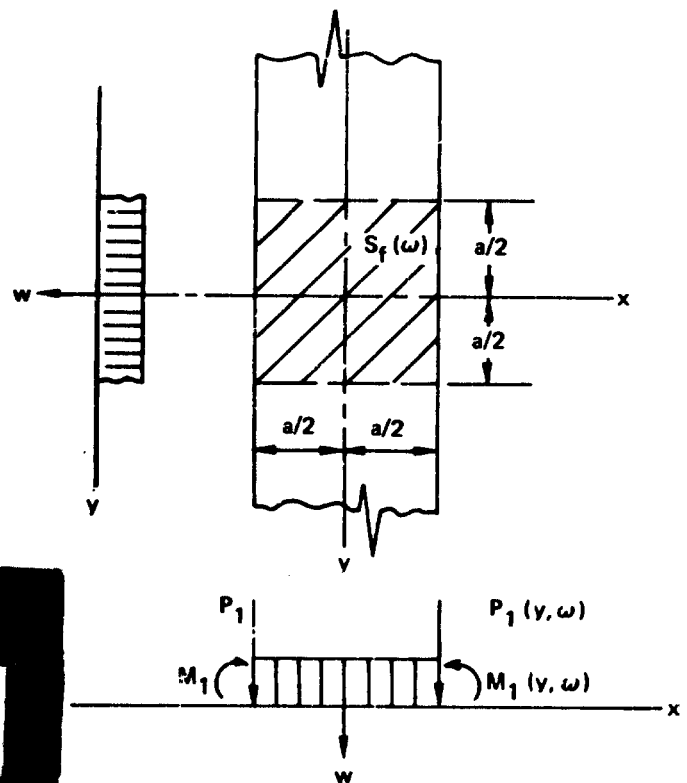

(a) AN INFINITE STRIP

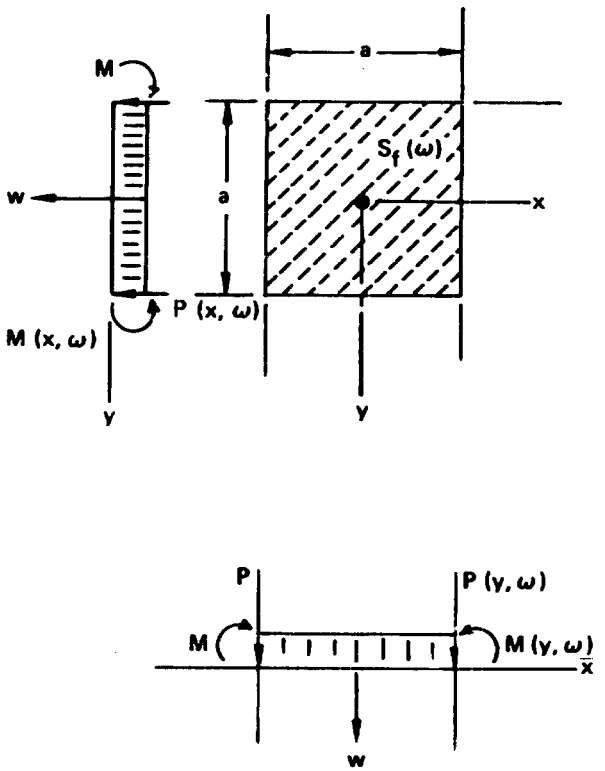

(b) A FINITE PLATE

FIGURE 15. AN INFINITE PLATE STRIP AND A SQUARE PLATE UNDER RANDOM ACOUSTIC LOADS